# FROM CLUSTER PROPERTIES TO CONCENTRATIONS AND FROM CONCENTRATIONS TO CLUSTER PROPERTIES

OONA KUPIAINEN-MÄÄTTÄ

Division of Atmospheric Sciences
Department of Physics
Faculty of Science
University of Helsinki
Helsinki, Finland

Academic dissertation

*To be presented, with the permission of the Faculty of Science
of the University of Helsinki, for public criticism in auditorium E204,
Gustaf Hällströmin katu 2, on May 27th, 2016, at 10 o'clock in the morning.*

**Helsinki 2016**

Author's Address:   Department of Physics
P.O. Box 64, FI-00014 University of Helsinki
e-mail: oona.kupiainen@alumni.helsinki.fi

Supervisors:   Professor Hanna Vehkamäki, Ph.D.
Department of Physics
University of Helsinki

Ismael K. Ortega, Ph.D.
Department of Physics
University of Helsinki
(Currently at ONERA, the French Aerospace lab)

Docent Theo Kurtén, Ph.D.
Department of Chemistry
University of Helsinki

Reviewers:   Professor Einar Uggerud, Ph.D.
Department of Chemistry
University of Oslo

Extra-ordinary associate professor Lauri Laakso, Ph.D.
Finnish Meteorological Institute

Opponent:   Professor Ian Ford, Ph.D.
Department of Physics & Astronomy
University College London

# Acknowledgements

I first came to the university planning to become a chemistry teacher, but I soon decided that everything I was learning was so interesting that it might be nice to stay in the academic world and become a researcher. I got my first scientific summer job already after my second year in Prof. Lauri Halonen's group in the Laboratory of Physical Chemistry, and I want to thank him, my other supervisors Elina Sälli (now Sjöholm) and Delia Fernándes-Torre, and the whole group for two very nice and instructive summers. I learned a lot about quantum chemistry, classical electrostatics and writing articles. Next I wish to thank Dr. Ari Harju for giving me the opportunity to do my Master's thesis in his Quantum Many-Body Physics group at the Helsinki University of Technology. There I got my first glimpse into developing new computational approaches for solving physics problems, and it was also interesting to see how life is at a different university.

After these first excursions into the scientific world, I heard from Dr. Theo Kurtén that Prof. Hanna Vehkamäki's group was doing interesting research that combined quantum chemistry with physics and was related to the atmosphere. This sounded captivating, and I was very happy to get a PhD student position in Hanna's group at the Department of Physics of the University of Helsinki. I would like to thank Theo for the tip, the heads of department Prof. Juhani Keinonen and Prof. Hannu Koskinen for providing the working facilities, the Väisälä foundation for two years of funding, CSC – IT Center for Science Ltd. for computer resources, Dr. Lauri Laakso and Prof. Einar Uggerudd for reviewing my thesis, and especially Hanna Vehkamäki for the opportunity to work in her group, for all her guidance and research ideas, for supporting me in various fights about research ethics, for letting me supervise summer students, *et cetera*.

The Computational Aerosol Physics group wouldn't exist without Hanna, but it also wouldn't be such a great place to work without the rest of the nice group members. I want to thank all my office mates (Tinja, Kai, Narcisse, Ville, Paula, Matti, . . . ), lunch companions (Kenty, Henning, Matti, Ville, Roope, . . . ), co-authors (Tinja, Hanna, Kenty, Theo, Kai, Henning, Noora, . . . ), supervisors (Hanna, Kenty, Theo), quantum chemistry workforce (Kenty, Henning) and other colleagues. A special thanks goes to my (apparently) look-alike Tinja Olenius for our seamless collaboration in developing ACDC and for many inspiring conversations about thermodynamics, cluster populations and other topics.

Finally, I wish to thank my husband Jussi for consoling and supporting me when I was most fed up with the realities of the academic world, on the other hand not complaining very much when I was working on something interesting and wanted to stay late at the office, and all in all being such great company.

Oona Katariina Kupiainen-Määttä (née Kupiainen)
University of Helsinki, 2016

**Abstract**

A large fraction of atmospheric aerosol particles are formed from condensable vapors in the air. This particle formation process has been observed to correlate in many locations with the sulfuric acid concentration, but the very first steps of cluster formation have remained beyond the reach of experimental investigation until recently. Charged clusters can now be detected and characterized starting from the smallest sizes and even neutral clusters consisting of only a few molecules can be detected, although their composition cannot be fully characterized. However, measuring the concentrations of different cluster types does not tell the full story of how the clusters were formed, and detailed simulations are needed in order to get a full understanding of the cluster formation pathways.

Cluster formation is described by a set of nonlinear differential equations that cannot be solved analytically in any realistic situation. The best way to understand the complex behavior of cluster populations is by cluster kinetics simulations. The focus of this Thesis is on developing tools for simulating cluster formation, and using the simulation results to improve the detailed understanding of atmospheric aerosol particle formation.

As sulfuric acid has been identified as the main driving force of cluster formation in many locations, it is also the main compound in the simulations of this Thesis. It cannot explain the observed atmospheric particle formation rates alone, and other possible participating species considered in this Thesis are ammonia, dimethylamine and water.

In the first two papers of the Thesis, theoretical values are used for the collision and evaporation rates, and simulated cluster concentrations and formation rates are compared to experimental observations. The simulation results agree well with experimental findings from two very different studies. The third and fourth paper asses existing methods for interpreting cluster measurements and point out details that should be taken into account: the effect of dipole moments on chemical ionization of neutral molecules and clusters, and the conditions for the widely used nucleation theorem to be valid. The last paper introduces a new method for extracting cluster evaporation rates from measured cluster distributions.

Keywords: atmospheric aerosols, molecular clusters, kinetic modeling, quantum chemistry, nucleation, sulfuric acid

# Contents

## List of publications

This Thesis consists of an introductory review, followed by five research articles. In the introductory part, these papers are cited according to their roman numerals.

**I** **O. Kupiainen**, I.K. Ortega, T. Kurtén and H. Vehkamäki. Amine substitution into sulfuric acid – ammonia, *Atmos. Chem. Phys.*, 12, 3591–3599, (2012).

**II** J. Almeida, S. Schobesberger, A. Kürten, I. K. Ortega, **O. Kupiainen-Määttä**, A. P. Praplan, A. Adamov, A. Amorim, F. Bianchi, M. Breitenlechner, A. David, J. Dommen, N. M. Donahue, A. Downard, E. Dunne, J. Duplissy, S. Ehrhart, R. C. Flagan, A. Franchin, R. Guida, J. Hakala, A. Hansel, M. Heinritzi, H. Henschel, T. Jokinen, H. Junninen, M. Kajos, J. Kangasluoma, H. Keskinen, A. Kupc, T. Kurtén, A. N. Kvashin, A. Laaksonen, K. Lehtipalo, M. Leiminger, J. Leppä, V. Loukonen, V. Makhmutov, S. Mathot, M. J. McGrath, T. Nieminen, T. Olenius, A. Onnela, T. Petäjä, F. Riccobono, I. Riipinen, M. Rissanen, L. Rondo, T. Ruuskanen, F. D. Santos, N. Sarnela, S. Schallhart, R. Schnitzhofer, J. H. Seinfeld, M. Simon, M. Sipilä, Y. Stozhkov, F. Stratmann, A. Tomé, J. Tröstl, G. Tsagkogeorgas, P. Vaattovaara, Y. Viisanen, A. Virtanen, A. Vrtala, P. E. Wagner, E. Weingartner, H. Wex, C. Williamson, D. Wimmer, P. Ye, T. Yli- Juuti, K. S. Carslaw, M. Kulmala, J. Curtius, U. Baltensperger, D. R. Worsnop, H. Vehkamäki, and J. Kirkby. Molecular understanding of sulphuric acid–amine particle nucleation in the atmosphere. *Nature*, 502, 359–363, (2013).

**III** **O. Kupiainen-Määttä**, T. Olenius, T. Kurtén and H. Vehkamäki. CIMS Sulfuric Acid Detection Efficiency Enhanced by Amines Due to Higher Dipole Moments: A Computational Study, *J. Phys. Chem. A*, 117, 14109–14119, (2013).

**IV** **O. Kupiainen-Määttä**, T. Olenius, H. Korhonen, J. Malila, M. Dal Maso, K. Lehtinen and H. Vehkamäki. Critical cluster size cannot in practice be determined by slope analysis in atmospherically relevant applications, *J. Aerosol Sci.*, 77, 127–144, (2014).

**V** **O. Kupiainen-Määttä**. A Monte Carlo approach for determining cluster evaporation rates from concentration measurements, *Atmos. Chem. Phys. Discuss.*, doi:10.5194/acp-2016-168, (2016).

# 1 Molecular clusters in the atmosphere

When thinking about the composition of the atmosphere, a good first approximation is to say that air is a 4:1 mixture of nitrogen and oxygen molecules. The biosphere also both needs and produces carbon dioxide and water vapor. This is, however, still not the whole picture, but instead around 1% of the air is made up of other nonreactive gases such as argon, and there are also trace amounts of reactive compounds such as sulfuric acid, ammonia and amines. Furthermore, air is not simply a homogeneous mixture of various gases. Practically everywhere in the atmosphere, tiny aerosol particles are suspended in the gas-phase. While notably bigger than individual nitrogen and oxygen molecules, these particles ranging up to a size of about 0.1 mm are nevertheless small enough not to fall immediately to the ground. Finally, in addition to electrically neutral molecules, clusters and particles, there are also positively and negatively charged ions in the air.

Atmospheric aerosol particles can be divided into two categories based on how they have entered the atmosphere. Primary particles such as pollen, desert dust and soot from biomass burning have first become particles and then been suspended in the air. Secondary particles, on the other hand, are formed in the atmosphere from gas-phase molecules. When two nitrogen or oxygen molecules collide with each other, they bounce off immediately. Some of the trace gas molecules present in very small quantities may instead stick together to form a cluster when they collide. These clusters may stay together simply due to intermolecular interactions, or a proton can transfer from one molecule to the other leading to the formation of a more strongly bound ion pair. If the cluster survives long enough before breaking back into the constituent molecules, a third suitable molecule might collide and stick to the cluster. Step by step, the cluster can then grow to a size comparable to the primary particles.

Although aerosol particles constitute only a very small fraction of the atmosphere, they have a significant effect on the climate (IPCC, 2013). They cool the planet both directly by scattering radiation and indirectly through changes in cloud properties, but the magnitude of these effects is rather poorly known. Some particles also heat the atmosphere by absorbing radiation, but the net effect is cooling. While the sources of primary particles can be inferred based on the composition of the particles and by following wind trajectories, the formation mechanisms of secondary particles have remained beyond the reach of direct experimental inves-

tigation until very recently.

Sulfuric acid was suggested as a likely key compound for particle formation in many locations (Doyle, 1961; Kiang et al., 1973; Cox, 1973; Mirabel and Katz, 1974) already before the Chemical Ionization Mass Spectrometer (CIMS) introduced by Munson and Field (1966) enabled field measurements of vapor-phase sulfuric acid concentrations (Arnold et al., 1981; Viggiano and Arnold, 1981; Eisele and Tanner, 1993). Correlations between the sulfuric acid concentration and the concentration of small particles consisting of some hundreds or thousands of molecules supported the idea of sulfuric acid–induced particle formation (Weber et al., 1995; Sihto et al., 2006), but the first steps of the process could still not be observed directly.

In the past few years, this gap has finally been bridged by the development of several new instruments. High-resolution, high-sensitivity mass spectrometers can detect and characterize individual charged clusters at ambient concentrations (Junninen et al., 2010). Using chemical ionization, also electrically neutral clusters consisting of only a few molecules can be detected (Zhao et al., 2010; Jokinen et al., 2012). However, although the smallest clusters can now be detected, the processes leading to their formation cannot be understood based on experiments alone.

The focus of this Thesis has been on developing theoretical and computational tools for studying the first steps of cluster formation. Initially, the main aims were to

- develop a procedure for simulating cluster formation based on theoretical estimates for collision and evaporation rate constants (**Papers I and II**)

- validate the methodology by comparing simulation results with experiments related to sulfuric acid–driven cluster formation (**Papers I and II**) and

- provide predictions for processes that cannot be or have not been measured directly (**Papers I and II**).

In order to understand the discrepancies between the simulations and measurements in **Paper II**, the objectives in the subsequent papers were to

- improve the understanding of instruments used in field measurements and particle formation experiments (**Papers III and V**)

- improve the understanding of data analysis methods applied to measurement data (**Paper IV**) and

- develop methods for determining cluster energies (**Paper III**) and rate constants (**Paper V**) directly from measurements.

# 2 From microscopic properties of clusters to observable quantities

The first part of this Introduction presents tools for modeling cluster populations. The aim is to start from the properties of individual clusters, find rate constants for collision and evaporation processes between the clusters, and finally solve the time-evolution of the cluster concentrations at some given conditions.

The first task is to decide which clusters are considered, and then find all the processes in which each of these clusters can be formed or lost. These formation and loss processes can be written down as birth-death equations

$$
\begin{aligned}
\frac{\mathrm{d}C_k}{\mathrm{d}t} \;=\; & \sum_{i,j\,|\,i+j\to k} \left( \beta_{i+j\to k} C_i C_j - \gamma_{k\to i+j} C_k \right) \\
& + \sum_{i,l\,|\,i+k\to l} \left( -\beta_{i+k\to l} C_i C_k + \gamma_{l\to i+k} C_l \right) \\
& + S_k - L_k C_k \,,
\end{aligned}
\tag{1}
$$

where $C_k$ is the concentration of cluster type $k$, $t$ is time, $\beta_{i+j\to k}$ is the collision rate of clusters $i$ and $j$ to form $k$, $\gamma_{k\to i+j}$ is the evaporation rate of cluster $k$ to form $i$ and $j$, $S_k$ is an external source rate for feeding cluster $k$ into the system and $L_k$ is an external loss term removing cluster $k$ from the system. The first summation goes over all pairs of clusters that can collide to form the cluster type $k$, while the second summation goes through all pairs of clusters $i$ and $l$ where $i$ can collide with cluster $k$ to form $l$. In a one-component system, the cluster labels can be set to correspond to the number of molecules in each cluster, and the birth-death equations get a simpler form by noting that $j = k - i$ and $l = k + i$. Also in a multicomponent case, indices $j$ and $l$ are uniquely defined by indices $k$ and $i$, and therefore from here on the collision rate between clusters $i$ and $j$ is denoted simply as $\beta_{i,j}$, and the notation for the evaporation rates is shortened from $\gamma_{k\to i+j}$ to $\gamma_{i,j}$.

Knowing the form of the birth-death equations is not enough – the next task is to find estimates for the rate constants. This is discussed in detail in Sections 2.2 and 2.3 after a short introduction to the main compounds of interest in Section 2.1. Finally, the differential equations need to be solved. In very simple cases this can be done analytically, but most often the only possibility is to integrate the equations numerically. Some details related to the cluster population simulations are

presented in Section 2.4, and the simulation results are compared to experiments in **Papers I and II**.

## 2.1   The studied compounds

While the discussion in Sections 2.2–2.4 is mostly presented on a general level, the main focus of the Thesis is on sulfuric acid–driven cluster formation in atmospherically relevant conditions. Sulfuric acid ($H_2SO_4$) is a strong acid formed in the atmosphere from sulfur dioxide. In polluted cities, its concentration in the air can be as high as $10^8$ cm$^{-3}$, but it has also been observed in boreal forests and other remote locations at concentrations around $10^5$ or $10^6$ cm$^{-3}$ (see **Paper II** and references therein).

Sulfuric acid is not the only compound involved in the formation of secondary aerosol particles in the atmosphere. Water vapor is always present in the air and participates in sulfuric acid cluster formation, but even sulfuric acid and water together do not form particles at a high enough rate to explain the observed concentrations of secondary aerosol particles in the boundary layer. Instead, some additional compound is needed to stabilize the clusters. This Thesis focuses on base molecules and ions as stabilizing compounds, and clusters containing sulfuric acid (**Papers I–V**), ammonia (**Papers I–V**), dimethylamine (**Papers I–IV**), ions (**Papers I–V**) and water (**Papers II and III**) are considered.

Ammonia ($NH_3$) and dimethylamine ($(CH_3)_2NH$, often referred to as DMA) are base molecules encountered in many locations in the atmosphere. Some of their main sources are animal husbandry, fish processing and industry, but there are also natural sources such as vegetation and oceans (Ge et al., 2011). Ammonia and DMA are often present in the atmosphere at ppt levels, but close to some anthropogenic sources their concentrations can be much higher.

Clusters can form through processes involving only electrically neutral molecules (**Papers II–IV**), but in some cases ionic clusters may provide a more favorable formation pathway (**Papers II, IV and V**). Atmospheric ions are formed when high-energy particles either from cosmic rays (Mohnen, 1970) or radon decay (Wilkening, 1985) collide with nitrogen and oxygen molecules. At sea level, the ion production rate is approximately 10 cm$^{-3}$s$^{-1}$ (Wilkening, 1985). The ions are lost by recombination when they collide with ions of opposite polarity, but before

that they can participate in cluster formation if cluster-forming compounds such as sulfuric acid are available at high enough concentrations. However, the rate of ion-induced cluster formation cannot exceed the ion production rate.

In small sulfuric acid–ammonia or sulfuric acid–DMA clusters, the base molecules act as a Lewis bases donating a free electron pair of the nitrogen atom to form a bond with an acid molecule. In larger acid-base clusters or hydrated clusters, sulfuric acid molecules can also act as a Brønsted-Lowry acids and donate a proton to an ammonia, DMA or water molecule.

## 2.2 Collision rates

The simplest way to get an estimate for collision rates is to use kinetic gas theory and assume that the molecules and clusters are hard spheres moving at velocities following the Maxwell-Boltzmann distribution

$$F(\boldsymbol{v}_i) = f(v_i) = \left( \frac{m_i}{2\pi k_\mathrm{B}T} \right)^{3/2} \exp \left( -\frac{m_i v_i^2}{2k_\mathrm{B}T} \right) , \tag{2}$$

where $\boldsymbol{v}_i$ and $v_i$ are the velocity and speed of the molecule or cluster $i$, respectively, $m_i$ is its mass, $k_\mathrm{B}$ is the Boltzmann constant and $T$ is the temperature. A collision occurs when the distance between the centers of two particles is equal to the sum of their radii.

Let us first consider a case where particle 1 with radius $r_1$ is moving at a speed $u$ and all particles of kind 2 are stationary and have a radius $r_2$. If the particles of type 2 have a number concentration $C_2$, the mean free path $l$ that particle 1 can on average move before colliding with one of them is

$$l = ut = \frac{u}{\beta_{1,2}^0 C_2} , \tag{3}$$

where $t$ is the average time between collisions and $\beta_{1,2}^0$ is the collision frequency between particles of types 1 and 2 in this setup. On the other hand, if particle 1 can on average travel a distance $l$ without colliding, there must on average be exactly one particle of kind 2 in the volume of the cylinder shown in Figure 1, and the concentration $C_2$ can be solved in terms of the mean free path as

$$C_2 = \left[ \pi \left( r_1 + r_2 \right)^2 l \right]^{-1} . \tag{4}$$
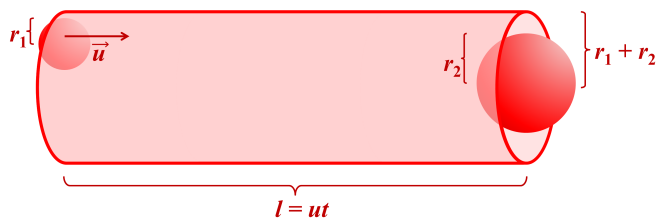
6

Figure 1: Schematic of a particle moving at speed $u$ before colliding with a stationary particle. The radii of the particles are $r_1$ and $r_2$ and the time before the collision happens is $t$.

Combining Eqs. (3) and (4) gives the collision frequency

$$\beta_{1,2}^0(u) = \pi \left(r_1 + r_2\right)^2 u \tag{5}$$

as a function of speed $u$.

The above discussion can be generalized to a case where both colliding particles are moving. For each pair of particles 1 and 2 moving at velocities $\boldsymbol{v}_1$ and $\boldsymbol{v}_2$, only the relative velocity $\boldsymbol{u} = \boldsymbol{v}_1 - \boldsymbol{v}_2$ is needed for determining whether and how soon the particles collide. The collision frequency can be calculated similarly as above for all pairs of velocities $\boldsymbol{v}_1$ and $\boldsymbol{v}_2$, and the overall collision frequency is obtained as an average over the velocity distributions,

$$\beta_{1,2} = \langle \beta_{1,2}^0(u) \rangle = \pi \left(r_1 + r_2\right)^2 \langle u \rangle . \tag{6}$$

The magnitude of the relative velocity for given $\boldsymbol{v}_1$ and $\boldsymbol{v}_2$ is

$$u = \left(v_1^2 + v_2^2 - 2v_1 v_2 \cos\theta\right)^{1/2} ,$$

where $\theta$ is the angle between velocities $\boldsymbol{v}_1$ and $\boldsymbol{v}_2$. By choosing suitable spherical coordinate systems for the velocities and using the speed distributions from Eq. (2), the mean relative speed can be calculated as

$$
\begin{aligned}
\langle u \rangle &= 8\pi^2 \int_0^\infty \mathrm{d}v_1 v_1^2 f(v_1) \int_0^\infty \mathrm{d}v_2 v_2^2 f(v_2) \int_0^\pi \mathrm{d}\theta \sin\theta \left(v_1^2 + v_2^2 - 2v_1 v_2 \cos\theta\right)^{1/2} \\
&= \left(\frac{8k_\mathrm{B}T}{\pi m_\mathrm{red}}\right)^{1/2} ,
\end{aligned}
$$

where $m_\mathrm{red} = m_1 m_2 / (m_1 + m_2)$ is the reduced mass of the pair of particles. The collision frequency is thus

$$\beta_{1,2} = (8\pi k_\mathrm{B}T)^{1/2} \left(r_1 + r_2\right)^2 \left(\frac{1}{m_1} + \frac{1}{m_2}\right)^{1/2}$$

7

for two noninteracting spherical particles. This approach has been used in **Papers I–IV** for all collisions between two neutral species, and the radii have been calculated based on bulk liquid densities.

### 2.2.1 Collision rates for interacting particles

In reality, particles may interact with each other already before they collide. Taking such interactions into account is crucial especially when one or both of the particles are electrically charged.

Let us first consider the case where one of the particles is an ion and the other is electrically neutral. The interaction potential can be approximated as (Moran and Hamill, 1963; Dugan and Magee, 1967)

$$V(\boldsymbol{r}, \psi) = -\frac{\alpha q^2}{8\pi\varepsilon_0 r^4} - \frac{\mu_{\mathrm{D}} q \cos\psi}{4\pi\varepsilon_0 r^2} \, , \tag{7}$$

where the two terms on the right-hand side correspond to the ion–induced dipole and ion–permanent dipole interactions, $\mu_{\mathrm{D}}$ and $\alpha$ are the dipole moment and polarizability of the neutral particle, respectively, $\psi$ is the angle between the dipole and the vector $\boldsymbol{r}$ separating the particles, $q$ is the charge of the ion, $\varepsilon_0$ is the vacuum permittivity, and all higher order terms such as dipole-dipole interactions are left out. The full equations of motion of the system containing both the relative motion of the particles and the rotation of the dipole in the electric field of the ion cannot be solved analytically, but two limiting cases are more simple (Moran and Hamill, 1963; Dugan and Magee, 1967). At one extreme, if the neutral molecule does not have a permanent dipole moment, only the ion–induced dipole term is left in Eq. (7) (Langevin, 1905). This simplified equation can also be used to approximate a situation where the rotation of the dipole is not affected at all by the electric field and this rotation is fast compared to the relative movement of the particles, so that the ion-dipole interaction averages out ($\langle\cos\psi\rangle = 0$). At the other extreme, the rotation of the dipole is suppressed completely and it remains in its lowest-energy orientation locked towards the ion ($\cos\psi = 1$). In both cases, what remains is a two-body central-force problem where the interaction potential depends only on the distance between the particles. A standard Lagrangian mechanics treatment yields for the locked-dipole case the effective radial potential

$$V_{\mathrm{eff}}(r) = \frac{L^2}{2m_{\mathrm{red}} r^2} - \frac{\alpha q^2}{8\pi\varepsilon_0 r^4} - \frac{\mu_{\mathrm{D}} q}{4\pi\varepsilon_0 r^2} \, , \tag{8}$$

8

where $L = m_{\text{red}}u_0 b$ is the angular momentum, $m_{\text{red}}$ is the reduced mass, $u_0$ is the relative speed at infinite separation and $b$ is the impact parameter giving the distance at which the particles would pass each other if their velocities did not change. The angular momentum term in the effective potential is the so-called centrifugal potential related to the acceleration required for changing the directions of the particles when they interact with each other. The case of the freely rotating dipole can be obtained from Eq. (8) by leaving out the last term or setting the dipole moment to zero, but let us first consider the more complicated locked-dipole case.

For a given value of the impact parameter $b$ and the initial relative speed $u_0$, the effective potential $V_{\text{eff}}(r)$ has one maximum at some inter-particle separation $r^*(b, u_0)$. Depending on the parameters $b$ and $u_0$, two outcomes are possible. If the initial relative kinetic energy is higher than the maximum of $V_{\text{eff}}(r)$, the particles overcome the barrier in the effective potential at separation $r^*$ and spiral towards each other until they collide. This is called a capture collision. A lower energy, on the other hand, leads only to a scattering where the direction of the particles changes before they reach the separation $r^*$. The cross-section for capture collisions is determined from the limiting value $b^*$ of the impact parameter where the maximum of the effective potential is equal to the initial relative kinetic energy. The cross-section depends on the initial relative kinetic energy, or equivalently the initial relative velocity, as

$$\sigma(u_0) = \pi b^{*2} = 2\pi \left[ \left( \frac{\alpha q^2}{4\pi \varepsilon_0 m_{\text{red}}} \right)^{1/2} \frac{1}{u_0} + \frac{\mu_{\text{D}} q}{4\pi \varepsilon_0 m_{\text{red}}} \frac{1}{u_0^2} \right]. \qquad (9)$$

Similarly as in Eqs. (5) and (6), the mean collision frequency is calculated by averaging the velocity-dependent frequency $u_0 \sigma(u_0)$ over all initial relative velocities (Gupta et al., 1967),

$$\beta_{\text{locked-dipole}} = \langle u_0 \sigma(u_0) \rangle = \frac{e}{2\varepsilon_0 m_{\text{red}}} \left[ (4\pi \varepsilon_0 \alpha)^{1/2} + \mu_{\text{D}} \left( \frac{2}{\pi k_{\text{B}} T} \right)^{1/2} \right], \qquad (10)$$

where the average $\langle 1/u_0 \rangle$ in the permanent dipole term is calculated assuming a Maxwell-Boltzmann velocity distribution for both the ion and the neutral particle. The collision rate for the case of a freely rotating dipole (Gioumousis and Stevenson, 1958) is obtained from Eq. (10) by leaving out the second term.

Collision rates are typically measured by studying reactions that can be assumed to occur at every collision. This is not quite straightforward, however, as there is

no way to confirm that a reaction is perfectly collision-limited, and on the other hand some reactions can happen through tunneling even if the reactants do not collide. Su and Bowers (1973) studied experimentally the reaction rates of ions with different isomers of difluorobenzene and difluoroethylene. As the studied isomers were essentially identical except for their dipole moment, the dipole moment dependence could be extracted from the results. The effect of the ion–permanent dipole interaction was observed to be between the two extremes discussed above, and the authors introduced the average-dipole-orientation (ADO) collision rate parameterization

$$\beta_{\mathrm{ADO}} = \langle u_0 \sigma(u_0) \rangle_{\mathrm{ADO}} = \frac{e}{2\varepsilon_0 m_{\mathrm{red}}} \left[ (4\pi\varepsilon_0\alpha)^{1/2} + c\mu_{\mathrm{D}} \left( \frac{2}{\pi k_{\mathrm{B}} T} \right)^{1/2} \right], \qquad (11)$$

where the permanent dipole term of Eq. (10) is multiplied by the parameter $c$ that they fitted to experimental data. They also postulated that the parameter could be interpreted as $c = \cos\langle\psi\rangle$ where $\langle\psi\rangle$ is the average angle between the orientation of the dipole and the vector $\boldsymbol{r}$ separating the particles. However, as noted by Barker and Ridge (1976), this interpretation does not seem sensible since the quantity to be averaged should be $\cos\psi$ and not $\psi$, and the result should depend on the separation $r$. Furthermore, it is not clear that the coupling between the rotation of the dipole and the relative translational motion of the two particles can be ignored. Despite these problems with the original interpretation of the parameterization, it was used in **Papers I–III** due to its good agreement with measured collision rates. The underlying assumption of point-like particles in the ADO theory may, however, cause problems for some collisions. When the colliding clusters are large and the electrically neutral collision partner has a very low dipole moment and polarizability, the ADO collision rate may be lower than the hard sphere collision rate computed from the cluster sizes. In **Papers I–III**, this problem was solved simply by using the hard sphere collision rate whenever it was higher than the ADO collision rate, but also more sophisticated solutions have been suggested (Kummerlöwe and Beyer, 2005).

Another approach for obtaining collision cross-sections is to simulate colliding and non-colliding trajectories by solving numerically the classical equations of motion of the particles (Dugan and Magee, 1967; Chesnavich et al., 1980; Su and Chesnavich, 1982). Extensive statistics for different values of initial velocities, rotational frequencies and impact parameters are required for calculating the average cross-section. Chesnavich et al. (1980) and Su and Chesnavich (1982) studied

the dependence of the cross-section on the dipole moments, polarizabilities and masses of the collision partners, and formulated a parameterization based on their trajectory simulations. This parameterization was used in **Papers III–V**.

For most of the collisions used in **Papers I–V**, the parameterizations of Su and Bowers (1973) and Su and Chesnavich (1982) both predict enhancement factors between one and ten compared to the kinetic gas theory value. The ion-neutral collision rates vary strongly between clusters with a similar size but different composition (**Paper III**). Especially acid-base clusters with an ion pair structure have a high dipole moment, leading to a high collision rate with ions.

An extreme case of collisions between interacting particles are those between ions of opposite polarity. These have received much less attention than ion-neutral collisions until very recently (López-Yglesias and Flagan, 2013; Franchin et al., 2015). In all **Papers II, IV and V** where recombination reactions are included, a fixed size-independent recombination rate constant (Israël, 1970) was used, corresponding to an enhancement factor of 2000–5000 compared to hard-sphere collisions.

At the other extreme are dipole-dipole interactions and other attractive forces between two neutral molecules or clusters. Based on their relatively short range, these interactions have been assumed, in the work presented in this Thesis, to have a negligible effect on collision rates. However, both experimental observations (Fuchs and Sutugin, 1965) and theoretical estimates (Marlow, 1980) suggest that the collision rate enhancement factor for two neutral nanometer-scale particles may, in fact, be as high as two or three – that is, quite comparable to ion-neutral enhancement factors. On the other hand, the derivation of Marlow (1980) is very different from that presented in Eqs. (7–10) for ion-neutral collisions, and it is not clear whether the estimates given by the two methods should be compared directly.

### 2.2.2   Sticking factors

The collision rates discussed above describe simply the frequency at which molecules and clusters get in contact with each other. It may then be asked, whether all such events lead to the formation of a cluster, even for a short time. It seems, for instance, plausible that clusters containing molecules with bulky hydrocarbon chains might not stick together if the collision geometry is such that only these nonreactive parts come in contact. However, there is at present no evidence

either way whether such collisions would stick or not. Loukonen et al. (2014a) used first-principles molecular dynamics to study head-on collisions of a pure or singly hydrated sulfuric acid molecule and a dimethylamine molecule, and found that irrespective of the initial collision geometry, the molecules always reoriented themselves into a configuration suitable for cluster formation. On the other hand, this might not necessarily be the case for collisions with larger impact parameters, higher initial kinetic energies or more inert groups on both collision partners. The effect of less-than-unity sticking factors was assessed in **Paper II** for simulations involving DMA. The relative change in particle formation rates and dimer concentrations was mostly larger than or equal to the relative change in the sticking factor, but depended on precursor concentrations.

Another possible cause for non-sticking collisions might be energy barriers in cluster formation processes. The product cluster would then only be formed if the collision partners had sufficient initial kinetic energy. Such kinetic barriers have been suggested some years ago by Bzdek et al. (2013) based on their experiments with positively charged sulfuric acid–ammonia clusters. A later quantum chemistry study on the same clusters (DePalma et al., 2014, 2015) confirmed that there might be energy barriers related to the reorganization of molecules to find the minimum energy configuration, but on the other hand the clusters were, in some cases, almost equally stable before rearrangement as in their optimal configuration. It seems, therefore, that sticking should not be seen strictly as an either-or question, but rather as a stepwise process where a collision results first in a moderately stable cluster that can then either stay together for some time, evaporate, or rearrange to a more favorable geometry. This more complex framework remains yet to be implemented in cluster formation simulations.

A third reason for some collisions not leading to cluster formation is related to excess energy. When two molecules or clusters collide and stick, the conservation of energy and momentum leads to some of the kinetic energy being dissipated as heat. More importantly, if cluster formation is energetically favorable, also some energy related to intermolecular interactions is released. This excess energy is taken up by the bonds in the formed cluster as vibrational energy, but if a vibrational degree of freedom related to cluster dissociation receives more energy than it can accommodate, the cluster may break up. Collisions with inert gas molecules that do not otherwise participate in cluster formation, including for instance nitrogen and oxygen, gradually cool the cluster to the ambient temperature, and as

the amount of excess energy diminishes, the probability of the cluster not surviving also decreases. In most of the collisions appearing in **Papers I–IV**, energy non-accommodation is expected not to be important due to the large number of vibrational modes (Kurtén et al., 2010). However, when the number of vibrational modes is small, like in the collision of two molecules, or if the amount of excess energy is very large, as is the case in collisions between positive and negative ions, energy non-accommodation may have a larger role.

## 2.3   Evaporation rates

There are, in principle, two approaches for obtaining theoretical estimates for evaporation rates. The direct way is to perform molecular dynamics (MD) simulations on the cluster of interest, and follow how long it takes for a molecule to evaporate from it. Román and Garzón (1991) and Weerasinghe and Amar (1991) have used this method for argon clusters, and determined the evaporation rates at different initial kinetic energies based on statistics gathered from a large number of simulation runs starting from different configurations. For argon clusters, the potential energy can be calculated very efficiently and quite accurately using pairwise Lennard-Jones interaction potentials, enabling the use of long simulation times. Román and Garzón (1991) used a simulation time of 0.2 $\mu$s, which was in this case long enough for all or almost all cluster configurations to evaporate at each value of the initial kinetic energy.

Atmospherically relevant clusters consist of multi-atomic molecules, not single rare-gas atoms, and simple classical interaction potentials cannot be used for calculating the potential energy. The most accurate method for directly simulating the fate of these clusters is to use first-principles MD and perform a quantum-chemical calculation at each time step. Loukonen et al. (2014b) used this approach to study sulfuric acid–ammonia and sulfuric acid–dimethylamine clusters. First-principles MD requires significantly more computer power than standard MD with classical interaction potentials, and the simulation runs of Loukonen et al. (2014b) were limited to 35 ps. None of the clusters evaporated during this timespan, and lengthening the simulation time by at least several orders of magnitude in order for the clusters to have time to evaporate is not, in practice, feasible. The simulations can be sped up by constructing classical interaction potentials based on quantum-chemical calculations, as has been done, for instance, by Stinson et al. (2016)

for sulfuric acid and water. However, these potentials need to be constructed separately for each pair of interacting molecule types, and as the procedure is complicated and time-consuming, this approach has not been widely used.

An alternative approach for calculating evaporation rates is to use the principle of detailed balance and the assumption that the evaporation rate is a fundamental property of each cluster and does not depend on the pressure or composition of the surrounding vapor, although it can vary with temperature. Furthermore, each cluster is assumed to be well represented by a single configuration and to have a well-defined constant energy. Based on these assumptions, each evaporation rate can be calculated in some equilibrium state and then generalized to be valid also in all other conditions at the same temperature.

If a reaction is in equilibrium, the flux from reactants to products must be equal to the reverse flux from products to reactants. More specifically, in the case of a cluster formation reaction $A + B \rightleftharpoons A \cdot B$, the collision flux

$$I_{\text{coll.}} = \beta_{A,B}^{\text{eff}} C_A^{\text{eq}} C_B^{\text{eq}} \tag{12}$$

from species A and B to form the cluster $A \cdot B$ must be equal to the evaporation flux

$$I_{\text{evap.}} = \gamma_{A,B} C_{A \cdot B}^{\text{eq}} \tag{13}$$

from $A \cdot B$ into A and B. In Eqs. (12) and (13), $C_A^{\text{eq}}$, $C_B^{\text{eq}}$ and $C_{A \cdot B}^{\text{eq}}$ are equilibrium concentrations of the colliding molecules or clusters and the collision product, respectively, $\beta_{A,B}^{\text{eff}}$ is the effective forward rate constant, and $\gamma_{A,B}$ is the evaporation rate constant of the cluster $A \cdot B$, corresponding to the frequency at which this cluster breaks up into species A and B. Assuming that each collision leads to the formation of the product cluster, the effective rate constant $\beta_{A,B}^{\text{eff}}$ in Eq. (12) is simply the collision rate constant discussed in Section 2.2. If, on the other hand, the colliding species stick together only when the collision occurs in a specific orientation, or if there is an energy barrier that needs to be overcome during the collision and evaporation processes, the forward flux (12) is lower than would be expected based on the collision rate constant as discussed in Section 2.2.2. The effective forward rate constant can then be written as $\beta_{A,B}^{\text{eff}} = k_{\text{stick}} \beta_{A,B}$, where the so-called sticking factor $k_{\text{stick}}$ is a number between zero and one. In order for the detailed balance condition to hold, the evaporation rate constant is also lowered by the sticking factor.

The equilibrium concentrations of each species are determined by the equilibrium constant $K_{\text{A,B}}$ through the law of mass action

$$K_{\text{A,B}} = \frac{(f_{\text{A·B}}^{\text{eq}}/p^{\ominus})}{(f_{\text{A}}^{\text{eq}}/p^{\ominus})(f_{\text{B}}^{\text{eq}}/p^{\ominus})} \, ,$$

where $f_i^{\text{eq}}$ is the fugacity of compound $i$ in an equilibrium mixture and $p^{\ominus}$ is the reference pressure. This expression can be simplified to

$$K_{\text{A,B}} \approx \frac{p^{\ominus}}{k_{\text{B}}T} \frac{C_{\text{A·B}}^{\text{eq}}}{C_{\text{A}}^{\text{eq}} C_{\text{B}}^{\text{eq}}} \tag{14}$$

by making the ideal gas assumption, which equates the fugacities to partial pressures and approximates the partial pressures in terms of concentrations $C_i$ as $p_i = k_{\text{B}}TC_i$. The equilibrium constant is related to the standard Gibbs free energy change for the reaction as

$$K_{\text{A,B}} = \exp\left(-\frac{G_{\text{A·B}}^{\ominus} - G_{\text{A}}^{\ominus} - G_{\text{B}}^{\ominus}}{k_{\text{B}}T}\right) \, , \tag{15}$$

where $G_i^{\ominus}$ is the Gibbs free energy of a single molecule or cluster $i$ when its partial pressure is $p^{\ominus}$.

Setting the forward and backward fluxes (12) and (13) to be equal and using Eqs. (14) and (15), the evaporation rate can be solved as

$$\gamma_{\text{A,B}} = \frac{p^{\ominus}}{k_{\text{B}}T} \beta_{\text{A,B}}^{\text{eff}} \exp\left(\frac{G_{\text{A·B}}^{\ominus} - G_{\text{A}}^{\ominus} - G_{\text{B}}^{\ominus}}{k_{\text{B}}T}\right) \, , \tag{16}$$

where $\beta_{\text{A,B}}^{\text{eff}}$ is typically taken to be the collision rate $\beta_{\text{A,B}}$, as there is no practical way for determining the sticking coefficients. The only remaining unknowns needed for computing the evaporation rate are then the Gibbs free energies of the molecules and clusters. As the pressure dependence of the Gibbs free energies is, within the ideal gas approximation, of the form $G(p) = G(p_0) + k_{\text{B}}T \log \frac{p}{p_0}$, the value obtained for the evaporation rate is independent of the choice of reference pressure. It should be noted that the energies are in the exponent in Eq. (16), meaning that even small inaccuracies in their values will lead to large errors in the evaporation rates. If some evaporation rates are close to the rates of other competing processes, small uncertainties in the corresponding energies can also lead to great uncertainties in cluster distributions as discussed in **Paper I**. Therefore, it is essential to obtain as accurate values as possible for the cluster formation energies.

15

A few different methods are available for assessing cluster energies. In principle, the most desirable approach would be to determine the energies experimentally, but such measurements are not straightforward and the most widely used methods have some caveats that are discussed in detail in Section 3.1. The simplest theoretical framework for calculating cluster energies is the classical liquid drop model (Volmer and Weber, 1926; Farkas, 1927; Becker and Döring, 1935). The classical liquid drop model is based on treating the clusters as spherical droplets of the bulk-phase liquid, and requires as input only the liquid density, molecular mass, surface tension and saturation vapor pressure of the compound. The drawback of this simple theory is that, while it may describe macroscopic droplets reasonably well, it is very inaccurate for the smallest clusters. It fails even for small argon clusters (Merikanto et al., 2007), and can be expected to perform even worse for substances with more complicated interactions. As liquid droplet energies are very quick to calculate and still have some physical foundation, they are convenient for studying general principles of cluster formation and growth (Olenius et al., 2014). However, they should not be used to draw any quantitative conclusions. Instead, cluster energies can be calculated more accurately using quantum chemical methods.

### 2.3.1 Cluster energies from quantum chemistry

Quantum chemistry refers to finding approximate solutions for the Schrödinger equation (Schrödinger, 1926)

$$\hat{H}\Psi = E\Psi \,, \tag{17}$$

where $\Psi$ is the wave function of the electrons and nuclei, $\hat{H} = \hat{K} + \hat{V}$ is the Hamiltonian consisting of a kinetic energy part $\hat{K}$ and a potential energy part $\hat{V}$, and $E$ is the energy eigenvalue corresponding to the state $\Psi$. Exact solutions can only be found for problems with one particle and a simple enough potential, but various schemes have been developed over the years for tackling more complicated problems with many nuclei and even more electrons. The first simplification to be made is the Born-Oppenheimer approximation, stating that due to the large difference in the masses of electrons and nuclei, the time scale related to electron motion is much shorter than the time scale of nuclear motion, and the wave function can be separated into a part corresponding to the electrons and a part corresponding to the atomic nuclei with negligible loss of accuracy. It is usually also assumed that the wave function of the nuclei is much less widely spread than that of the electrons, and that the nuclei are either located at their minimum energy configuration or

oscillate close to those positions. With these assumptions, the remaining task is to solve the electronic wave function and corresponding lowest energy eigenvalue with different configurations of the nuclei, add to this energy the contribution from the repulsion between the nuclei, and move the nuclei around to minimize the overall energy of the system.

Methods for solving the electronic part of the Schrödinger equation can be divided into two categories: wave function methods and density functional methods. The simplest wave function method is the Hartree-Fock (HF) method (or self-consistent field method), and it is also the basis for the more advanced wave function methods. Each electron is treated as moving alone in a potential determined by the electric fields of the stationary nuclei and the average field created by the other electrons. As the potential experienced by each electron depends on the wave function of all other electrons, and the wave functions, on the other hand, depend on these potentials, the equations need to be solved iteratively. The basic idea is to start from some set of wave functions for the electrons, compute the electron-electron interaction potentials, solve a new wave function for each electron, and continue the procedure until the potentials and wave functions no longer change. At each iteration, the eigenfunctions with lowest energies are selected, and at the end of the iteration process they are combined into a many-electron wave function corresponding approximately to the ground state of the system. The many-electron wave function is formed from the one-electron orbitals as a Slater determinant, in order to ensure antisymmetry with respect to the exchange of two electrons. In practice, the one-electron wave functions are constructed as linear combinations of a finite set of basis functions, and increasing the size of the basis set improves the accuracy of the results. The variational principle ensures that the ground-state energy obtained from a Hartree-Fock calculation is always an upper limit to the true ground-state electronic energy. However, even disregarding the error resulting from a finite basis set, the Hartree-Fock method does not give the true solution to the full many-electron problem because of the simplifications made in the description of electron-electron interactions. While the exchange interaction related to the antisymmetry of many-electron wave functions is taken properly into account by using a Slater determinant, the Coulomb interaction between electrons is only treated in an averaged way.

So-called post-Hartree-Fock methods build upon the results obtained from a Hartree-Fock calculation but attempt to overcome this deficiency. Some of the

commonly used methods include Møller-Plesset second order perturbation theory (MP2), configuration interaction methods (CI) and coupled cluster methods (CC). They all start by using the Hartree-Fock one-electron orbitals, both those appearing in the HF ground state many-electron wave function (occupied orbitals) as well as higher-energy one-electron wave functions corresponding to excited states (virtual orbitals), to construct a basis set of several many-electron wave functions. These many-electron wave functions can be classified according to how many electrons are excited from the Hartree-Fock ground state solution to some higher energy orbitals. Singly excited states refer to many-electron wave functions where one electron is in a virtual orbital, doubly excited states have two electrons in virtual orbitals and so on. In the MP2 method, these excited states together with the ground state are used as a basis set for calculating an energy correction using second order perturbation theory, while in the two other methods a many-electron wave function is constructed as a linear combination of these basis functions and is then inserted into the Schrödinger equation. The CI and CC methods differ in which excitations are included in this linear combination and how their coefficients are determined.

In density functional theory (DFT), the whole problem of solving the Schrödinger equation is reformulated so that the quantity to be solved is no longer the many-electron wave function but the total electron density. Electron-electron interactions are, in principle, inherently taken fully into account, but in practice the exact form of the functional describing them is not known. Instead, some approximation must be used, and different density functional methods employ different exchange-correlation functionals for computing the approximate electron-electron interaction energy based on the electron density. The exchange-correlation functional may depend either only on the electron density (local density approximation, LDA) or also on the gradient of the electron density (generalized gradient approximation, GGA), and hybrid functionals combine an LDA or GGA functional with the Hartree-Fock exact exchange energy. The electron density is expressed as the square sum of so-called Kohn-Sham orbital wave functions, and the equation for the energy as a functional of the electron density is transformed into Hartree-Fock-type equations for the Kohn-Sham functions. These Kohn-Sham equations are solved iteratively like in the Hartree-Fock self-consistent-field method. Once again, the one-electron functions are constructed as linear combinations of some set of basis functions, and solving the Kohn-Sham equations is equivalent to finding the best coefficients for the basis functions. In accordance with the variational principle, the DFT

energy is always higher or equal to the exact energy corresponding to the specific functional used. However, this energy can, in turn, be either lower or higher than the true electronic energy of the system. Therefore, the arguments showing that the HF energy is always an upper bound to the exact ground-state energy do not apply to DFT methods, despite the similarity between the Kohn-Sham equations and the Hartree-Fock equations.

The basis functions used in Hartree-Fock and DFT calculations are most often functions roughly corresponding to the atomic orbitals of each atom. The smallest possible basis set includes one spatial basis function for every two electrons, in practice those corresponding to the occupied orbitals in the free atoms, and for most atoms a few additional orbitals to ensure proper symmetry. In practice, instead of using only one basis function per orbital, additional basis functions with the same angular symmetry and same number of nodes in the radial direction but slightly different shape are typically used at least for the orbitals of the valence electrons of each atom. Also additional higher energy $p$- and $d$-type orbitals can be included to account for polarization of the valence orbitals when forming bonds.

Once the minimum energy geometry of the atomic nuclei has been found, their motion still needs to be examined. Also the movement of the nuclei needs to be treated using quantum mechanics, but doing this explicitly even for a few bonds gets very complicated (Partanen et al., 2012). Therefore, all vibrational degrees of freedom are usually approximated as uncoupled harmonic oscillators and the whole molecule or cluster is treated as a rigid rotor. After determining the curvature of the potential energy surface close to the minimum energy configuration, energy levels of the harmonic oscillators can be calculated analytically. Solving the energy levels of the rigid rotor only requires the moments of inertia calculated from the masses and coordinates of the nuclei. These energy levels can be used for computing the thermal energy related to rotations and vibrations at a given temperature. For small molecules, this rigid-rotor-harmonic-oscillator (RRHO) approach may be a reasonable approximation, although even then anharmonicities of the vibrations and couplings between different vibrations and between vibrations and rotations may be non-negligible. For clusters with stronger bonds within the molecules and weaker bonds between them, the approximation is less justified. In fact, a first-principles molecular dynamics study by Loukonen et al. (2014b) investigating some of the clusters used in this Thesis showed that the molecules rotated inside the clusters breaking inter-molecular bonds and forming new ones. How-

ever, if the aim is, as in this Thesis, to calculate reasonably reliable energies for a comprehensive set of clusters instead of calculating an extremely accurate energy for a single small cluster, the only feasible way for treating the nuclear motion is to use the RRHO approximation. While this approach is far from perfect, it is much better than neglecting the motion of the nuclei altogether.

Hartree-Fock is the most simple and, apart from semiempirical methods, computationally least demanding electronic structure method. On the other hand, it is also not very accurate, and is therefore most often used only as a starting point for more advanced wave function methods. The CI and CC methods approach the exact solution of the many-electron Schrödinger equation when all possible excitations are included, and they also give good results when only single, double and possibly triple excitations are used, which is in practice often done. The drawback of these methods is that they are computationally demanding and only applicable for small systems, especially when using more than doubly excited states. Furthermore, as the first task is to find the minimum energy configuration of the nuclei, a large number of electronic structure calculations needs to be performed with different positions of the nuclei before the optimal geometry is found. More optimization steps and also more optimization processes starting from different initial guesses will typically be required for larger systems, unfortunately making these best methods inapplicable for the clusters studied in this Thesis. DFT methods are far from being as accurate as the best post-Hartree-Fock wave function methods, but they still account for most of the electron correlation energy while being computationally much less demanding.

The cluster formation energies used in **Papers I–V** of this Thesis were mostly computed with a combination of lower- and higher-level quantum chemistry methods as described by Ortega et al. (2012). The cluster geometries were first optimized with DFT, using the B3LYP hybrid functional (Becke, 1993) and a CBSB7 basis set (Montgomery et al., 1999). The same method was also used for computing the harmonic frequencies for the vibrational motion of the nuclei around their minimum energy positions. An RI-CC2 calculation (Hättig and Weigend, 2000) with an aug-cc-pV(T+d)Z basis set (Dunning et al., 2001) was then performed for the configuration corresponding to the lowest energy at the B3LYP/CBSB7 level. The RI-CC2 method is an approximate version of CCSD, the coupled cluster method including single and double excitations, and its accuracy is typically between MP2 and CCSD. The RI-CC2 electronic energy was combined with the

lower-level RRHO thermal corrections to get an approximate Gibbs free energy for each molecule and cluster. The advantage of such combination methods is that the electronic energy is calculated with a higher level method than would be possible if the same method was used for the geometry optimization. As a drawback, the geometry used in the electronic energy calculation does not correspond to the optimal configuration at that level of theory. The error caused by this discrepancy is expected to cancel out when calculating stepwise energy changes between clusters of different sizes, but there is no guarantee for this to be the case.

In **Paper III**, three quantum chemical methods are used for computing cluster energies and evaporation rates: the combination method described above, a pure DFT method, and a higher level composite method combining different post-Hartree-Fock methods for calculating the electronic energy and using HF for the vibrational frequencies. These three sets of evaporation rates were used in cluster formation simulations, and the differences in the cluster distributions were found to be quite dramatic. Noting that different quantum chemical methods yield different cluster formation energies is not, in itself, a new finding, and more extensive method comparisons have been presented by Leverentz et al. (2013) and Elm et al. (2013). However, **Paper III** is the first study illustrating how these differences propagate to simulated cluster distributions. For some of the smaller electrically neutral clusters considered in the paper, the three quantum chemistry methods yielded Gibbs free energies of formation that were within 1.5 kcal/mol of each other, but already for the stepwise energy difference between the clusters containing two sulfuric acid molecules and one or two DMA molecules, the pure DFT method differed from the two other methods by 10 kcal/mol. This translates into a difference of seven orders of magnitude in the cluster lifetime (half a millisecond for the DFT method *vs.* more than an hour for the composite methods) and qualitative differences in predicted steady-state cluster distributions in some atmospherically relevant conditions. In the light of the findings of **Paper III**, it should be kept in mind that while quantum chemistry is the best theoretical approach for computing cluster energetics, it must not be expected to provide the absolute truth. In some situations, quantum chemical calculations may not even give a correct qualitative prediction for cluster concentrations. Furthermore, the reliability of different quantum chemistry methods has mostly been tested only for single molecules or crystal structures, and there is no way to asses conclusively their performance on loosely bound molecular clusters. On the other hand, in some special cases such as that discussed in **Paper I**, the predicted concentrations

may agree even quantitatively with measurements if the evaporation time scales of all clusters are either much shorter or much longer than the time scale of the experiment.

## 2.4 Cluster kinetics simulations

Performing cluster kinetics simulations is, at least in principle, very straightforward once the rate constants have been determined. The birth-death equations (Eq. 1) give the time derivative of each cluster concentration, and integrating the equations numerically with respect to time yields the time evolution of the cluster concentrations. One minor difficulty is that the system of differential equations is often stiff, but at least the ode15s solver (Shampine and Reichelt, 1997) for MATLAB used in **Papers I–IV** and the VODE routine (Brown et al., 1989) for Fortran used in **Paper V** are suitable tools for integrating the equations.

The most difficult task may, in fact, not be solving the equations but writing them out. Even a moderate number of clusters results in a large number of equations if all pairs of clusters can collide with each other, and writing the birth-death equations manually is time-consuming and error-prone. Ideally, the equations could be written using sums over all clusters, but the necessity of using a limited set of clusters complicates matters. The Atmospheric Cluster Dynamics Code (ACDC) used in **Papers II–V** has been devised to automate the generation of the differential equations taking these finite-size effects into account.

### 2.4.1 Consequences of a finite system size

In principle, the birth-death equations describe all possible collision and evaporation processes between all possible clusters up to arbitrarily large sizes. In practice, however, the equations can only be integrated for a finite set of clusters, and using quantum chemistry for evaluating the evaporation rates limits the studied cluster sizes further. Some collisions between species included in the system will then necessarily lead to the formation of clusters outside the studied set of clusters. If an evaporation rate is not available for the formed cluster, it is not clear what its fate will be. However, trends of the evaporation rates of clusters inside the system with respect to their composition may give a good indication. For instance, in sulfuric

acid–base cluster formation, the most stable clusters have a similar number of acid and base molecules, while pure base clusters and pure acid clusters are unstable (Olenius et al., 2013a).

If a collision leads to a cluster growing out of the system in an unfavorable direction, the produced cluster is more likely to evaporate back into the studied system than to grow further. For instance, if the collision of clusters A and B produces cluster C that is outside the studied system and expected to be unstable, if C is expected to be most likely to evaporate molecule D to form cluster E that is still beyond the limits of the system, and if E will most probably evaporate another molecule D and produce cluster F, which is one of the studied clusters, the simplified reaction $A + B \longrightarrow F + 2\,D$ can be used in the birth-death equations.

On the other hand, when collisions produce clusters that are outside the limits of the system but that are expected to have low evaporation rates, these should not be forcefully brought back to smaller sizes by removing molecules. Instead, such collisions contribute to the formation rate of stable big clusters, often referred to as the nucleation rate. In **Paper II**, the simulated particle formation rate defined in this way is compared to the experimental formation rate determined from measured particle concentrations. It should, however, be noted that these two definitions for the formation rate are not quite equivalent, and the good agreement in **Paper II** is partly coincidental.

### 2.4.2 Averaging over hydrate distributions

Including water vapor and hydrated clusters in cluster kinetics simulations of sulfuric acid–base cluster formation at atmospheric conditions increases the stiffness of the birth-death equations, and makes them in practice unsolvable even with the MATLAB ode15s solver designed specifically for stiff systems. The problems stem from the concentration of water vapor being around ten orders of magnitude higher than the concentrations of the other vapors, and on the other hand water molecules being very loosely bound to the clusters and having high evaporation rates. As a result, the time scale of all processes involving the addition and removal of water molecules is orders of magnitude shorter than the time scale of other growth, evaporation or loss processes. This division into two separate time scales can, however, be turned into an advantage by using a similar reasoning as in the Born-Oppenheimer approximation. All other processes happen so slowly

from the point-of-view of hydration processes that the hydrate distributions of all molecules and clusters can be assumed to relax to the equilibrium distribution immediately after any longer-time-scale process. Therefore, the individual hydrates do not need to be considered separately, but can instead be averaged over. Such an approach was first introduced for sulfuric acid–water nucleation by Shugard et al. (1974) using classical liquid droplet energies, but they only allowed collisions and evaporations of individual sulfuric acid and water molecules. Yu (2005) developed a different quasi-unary sulfuric acid–water model, where one hydration number corresponding to the lowest Gibbs free energy of formation is chosen for each number of sulfuric acid molecules, and only growth and evaporation processes along the sulfuric acid coordinate are considered. Later, the method was also extended to describe sulfuric acid–ammonia–water nucleation in a quasi-unary fashion (Yu, 2006). The original method of Shugard et al. (1974) does not allow the hydrates of sulfuric acid monomers to contribute to cluster growth, although they were found to dominate over dry sulfuric acid molecules in the studied conditions. The method of Yu (2005) fixes this problem, but still only considers the evaporation of bare sulfuric acid monomers. A third approach is to calculate collision and evaporation rates for all combinations of different hydration states for all participating clusters, and then average these over the hydrate distributions of the evaporating cluster or the two collision partners. This procedure was first introduced by Paasonen et al. (2012) and is used in **Paper II** to study the effect of relative humidity on sulfuric acid–dimethylamine particle formation rates.

# 3 From observations to microscopic properties of the clusters?

As has been discussed in the first part of this Introduction, theoretical predictions for rate constants can be validated by using them in cluster formation simulations and comparing the results with experimental findings. However, if the simulations and measurements do not agree, as is likely to happen, it is unclear what conclusions should be drawn. Is the problem in the simulations or in the measurements? If the error is in the simulations, could it be that only one cluster energy is slightly inaccurate, but the error propagates and, due to the highly nonlinear nature of the problem, has drastic effects on the simulation results? Or is it more likely that all collision rates are systematically wrong because of an insufficient understanding of intermolecular interactions?

In order to answer these questions, or completely avoid them, it would be useful to be able to determine the rate constants or other microscopic cluster properties directly based on measurements. Since the dependence of concentrations on rate constants cannot, in general, be described by a closed-form function that could be inverted to solve rate constants based on concentrations, the problem must be approached in a more roundabout way. Some relatively straight-forward but somewhat problematic approaches for determining cluster energies based on equilibrium concentrations are described in Section 3.1. The widely used slope analysis method devised for finding the highest-energy cluster along the formation pathway is presented in Section 3.2, and some flaws of the method pointed out in **Paper IV** are summarized in Section 3.2.2. Finally, Section 3.3 discusses some earlier attempts at determining rate constants by fitting a model to experimental data, and an extensive framework introduced in **Paper V** for determining all rate constants is presented in Section 3.3.2.

Attempts at determining rate constants or cluster energies from cluster measurements raise a whole new set of questions regarding the reliability of experimental results. What happens inside the instruments used for measuring cluster concentrations? How accurate is the conversion from instrument count rates to cluster concentrations? Are all clusters measured with the same detection efficiency? Does the composition of some clusters change in the instrument before they are detected? Also these questions are discussed briefly in Sections 3.1 and 3.3.

## 3.1  Cluster energies from equilibrium concentrations

For a cluster population at constant pressure and temperature, the appropriate energy quantity for comparing cluster stabilities is the Gibbs free energy of formation. If the system is in equilibrium, the concentrations follow the Boltzmann distribution

$$C_i^{\text{eq}} \propto \exp\left(-\frac{\Delta G_i}{k_{\text{B}}T}\right) , \tag{18}$$

where $C_i^{\text{eq}}$ is the concentration of molecule or cluster $i$, $\Delta G_i$ is its Gibbs free energy of formation, $k_{\text{B}}$ is the Boltzmann constant and $T$ is the temperature. Thus, by measuring cluster concentrations, it would be possible to solve directly the cluster formation free energies. An outline of the procedure is presented in Figure 2.

This approach has been used already in the 1960s for ionic clusters (Hogg and Kebarle, 1965; Kebarle and Hogg, 1965; Hogg et al., 1966), and is still the dominant method for experimental determination of cluster energies (Froyd and Lovejoy, 2003a,b, 2012). It has also been extended to neutral clusters by employing chemical ionization mass spectrometry (Hanson and Lovejoy, 2006) or infrared (IR) spectroscopy (Hippler, 2007; Bork et al., 2014a,b). There are, however, several caveats in the measurements and data analysis that must be considered. Most of these were actually discussed to some extent already in the very first papers (see for instance Hogg et al., 1966).

First of all, the cluster distribution must be in equilibrium. In other words, no larger particles are allowed to form. This can be achieved by using low enough vapor concentrations that while small clusters are formed, a barrier in the formation free energy surface inhibits effectively the formation of larger clusters. Even if some nucleation occurs, the steady-state size distribution of clusters below the
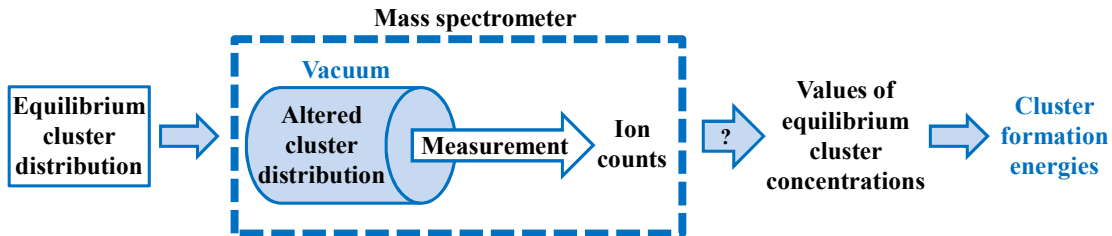


Figure 2: Outline of the process for obtaining cluster energies from a cluster distribution measurement.

critical size is close to the Boltzmann distribution (Yasuoka and Matsumoto, 1998) if the system exhibits a high energy barrier. In order for the system to reach equilibrium or a steady-state, the time that the clusters are allowed to grow before being either measured or lost on walls or, in case of ions, by recombination must be longer than their lifetime with respect to growth and evaporation processes (Hogg and Kebarle, 1965).

In case of hydrate distributions of ions, the requirement of reaching equilibrium is, in general, not a problem. Water has a high equilibrium vapor pressure, so high vapor concentrations can be used without worrying about nucleation. The high vapor concentration and high evaporation rates result in a short time scale for collision and evaporation processes, and the hydrate distribution is likely to be close to equilibrium regardless of any other processes such as external losses. The situation is more complicated for substances that form strongly bound clusters, as a high vapor concentration leads to particle formation and a too low vapor concentration enhances the effect of external losses.

Once the desired equilibrium cluster distribution has been produced, the next question is whether it can be measured. In the experiments where a mass spectrometer is used, the interface between the chamber where the clusters are formed and the instrument must be considered in detail. When a sample enters a mass spectrometer, it experiences a substantial pressure drop. Before entering the instrument, a dynamic equilibrium is maintained by molecules colliding with clusters at a rate equal to that of molecules evaporating from the clusters, but after the monomer concentration has been lowered by vacuum pumps, evaporation processes start to dominate. If the evaporation life times of the clusters are shorter than the residence time in the mass spectrometer, the clusters are detected at lower masses than what they had when they entered the mass spectrometer (Hogg and Kebarle, 1965). Fragmentation of the clusters can also be induced by energetic collisions with carrier gas molecules when the ions are accelerated (Hiraoka and Kebarle, 1975; Froyd and Lovejoy, 2003a, Adamov et al., 2013). On the other hand, in some experimental set-ups the sample is cooled adiabatically in the inlet of the mass spectrometer. This may lead to growth of the clusters if evaporation rates decrease with decreasing temperature faster than the monomer concentration decreases (Hogg and Kebarle, 1965). These processes cannot be completely eliminated, but the extent to which cluster sizes change in the inlet of the mass spectrometer can be varied by tuning flow rates, electric fields and other parame-

ters, and this can give some insight into the importance of these phenomena (Hogg and Kebarle, 1965; Hiraoka and Kebarle, 1975; Froyd and Lovejoy, 2003a).

Another issue related to measuring the cluster distribution with a mass spectrometer is the mass dependence of the transmission and detection efficiency of the instrument (Hogg and Kebarle, 1965; Ehn et al., 2011). The ion counts must, in principle, be converted to concentrations in order to obtain cluster energies. However, as only the concentration ratios between consecutive clusters are needed for determining step-wise formation energies, the effect of mass discrimination is often neglected on the basis that the counting efficiency does not differ much for two consecutive cluster sizes (Hogg and Kebarle, 1965; Froyd and Lovejoy, 2003a). A more sound approach is to convert the ion counts to concentrations using a mass-dependent transformation, but obtaining reliable conversion functions is far from trivial (Ehn et al., 2011). When neutral clusters are charged by chemical ionization before entering the mass spectrometer, differences in charging probabilities between the clusters (**Paper III**) add to the uncertainty in converting ion counts to concentrations, and changes in composition after ionization (**Paper III**, Ortega et al., 2014) complicate the assignment of the observed masses to the original neutral clusters.

Experiments based on IR spectroscopy avoid the problems related to sampling and fragmentation encountered when using a mass spectrometer, as the measurement can be performed in the same mixing cell where the clusters are produced (Hippler, 2007; Bork et al., 2014a,b). On the other hand, converting the signal into a cluster concentration requires the absorption coefficient of the cluster, which can only be obtained from quantum chemistry. Therefore, cluster energies determined from IR measurements are, in a sense, not purely experimental.

A different approach with regard to the transmission efficiency of different clusters through an instrument was introduced by Hanson and Eisele (2000). In their study, the fact that different clusters have different transmission probabilities through a flow reactor was not a problem to be solved or avoided, but instead the key to a new way of determining formation energies of neutral clusters. The effective sulfuric acid wall loss in a laminar flow tube was determined at different relative humidities by introducing sulfuric acid vapor in the flow tube and measuring its concentration with a Chemical Ionization Mass Spectrometer (CIMS) at different points along the tube. The CIMS was assumed to detect the plain acid molecule and its hydrates as bisulfate ions with identical efficiency. The sulfuric acid hydrate

distribution was solved from the overall wall loss of sulfuric acid based on the different diffusion limited wall loss constants of the plain acid molecule and its hydrates. The diffusion coefficients of the hydrates were estimated theoretically, leading to the drawback of also this method not being purely experimental.

A similar idea is taken further in the experiment proposed in **Paper III**. The method is based on acid-base clusters having a different detection efficiency than acid monomers in the CIMS, but now these efficiencies do not need to be known in advance. The total sulfuric acid concentration in an experiment chamber is kept constant, and the base concentration is varied over several orders of magnitude. The bisulfate signal in the CIMS is measured at each base concentration, and the point where it is halfway between its low-base and high-base limits gives the base concentration where half of the sulfuric acid molecules are clustered with a base molecule. This base concentration can be used to solve the Gibbs free energy of formation of the cluster. The only requirement is that the neutral molecules and clusters are close to equilibrium, or in practice in a steady state where collisions between acid and base monomers are much more frequent than any processes removing acid molecules or acid-base dimers from the experiment. Such losses include for instance deposition on walls. Also growth of clusters to larger sizes must be negligible, which means that the acid concentration must be low enough.

## 3.2 The critical cluster from the nucleation theorem

While the equilibrium distribution is the distribution best suited for solving cluster energies, reaching equilibrium is only possible in situations where clusters do not grow to large sizes. However, the main focus in the study of atmospheric particle formation has often been in understanding and quantifying the formation of particles large enough to act as cloud condensation nuclei. This requires a diameter of at least some tens of nanometers, corresponding to hundreds of thousands or millions of molecules.

The gas-to-liquid phase transition occurring when particles are formed from vapor-phase molecules has generally been assumed to proceed by nucleation. This means that the particle formation free energy surface has a barrier that has to be crossed before particle growth becomes energetically favorable. The cluster with the highest free energy of formation is called the critical cluster.

Theoretical research on first-order phase transitions and nucleation led to the discovery of the nucleation theorem (Nielsen, 1964; Kashchiev, 1982)

$$\left( \frac{\partial \log J}{\partial \log C} \right)_T \approx n^*  \tag{19}$$

relating the steady-state nucleation rate $J$, the precursor concentration $C$ and the critical cluster size $n^*$ at constant temperature $T$. This simple formula has given rise to a seemingly easy-to-use data analysis scheme often referred to as slope analysis. Particle formation rates are determined experimentally at different precursor concentration, the data is presented on a log-log scale, and the slope of a linear fit to the data points is interpreted as the critical size. An outline of the procedure is presented in Figure 3.
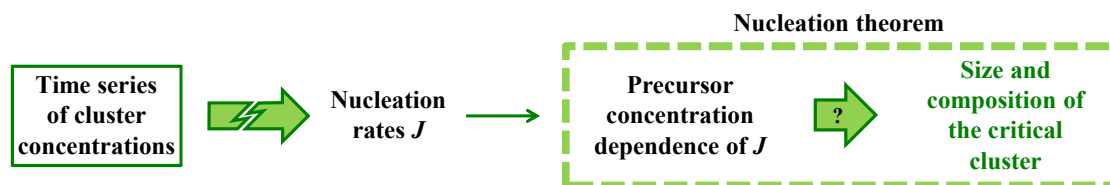


Figure 3: Outline of the process for solving the critical cluster size from particle formation experiments. Both steps, obtaining the nucleation rate and applying the nucleation theorem, are problematic.

### 3.2.1 The theory behind slope analysis

In the simplest case of a one-component system with no cluster-cluster collisions, no splitting of clusters into two non-monomer products and no external losses, the dynamics of the system is described by the Szilárd-Farkas scheme where the net fluxes between two consecutive cluster sizes are

$$I_k = \beta_{1,k} c_1 c_k - \gamma_{1,k} c_{k+1} \,,  \tag{20}$$

where $c_1$ is the monomer concentration of the vapor, $c_k$ and $c_{k+1}$ are the concentrations of clusters consisting of $k$ and $(k+1)$ molecules, respectively, $\beta_{1,k}$ is the collision frequency between the monomer and the $k$-molecule cluster, and $\gamma_{1,k}$ is the evaporation rate of a molecule from the $(k+1)$-molecule cluster. In equilibrium, the collision and evaporation fluxes would be in equal, resulting in the net flux being zero. Another special case is the steady-state where all concentrations are time-independent but there is a net flow through the system as clusters form

and grow to big sizes. The time derivative of each cluster concentration is zero, and can be expressed as

$$\frac{\mathrm{d}c_k}{\mathrm{d}t} = I_{k-1} - I_k = 0\,, \tag{21}$$

in terms of the fluxes to and from that cluster.

**Calculating d(log $J$)/d(log $C$)**

Following the reasoning of McGraw and Wu (2003), the steady-state formation rate can be solved from Eqs. (20) and (21) with the help of so-called "constrained equilibrium" concentrations $c_{k,0}$. These are defined through the detailed balance condition

$$\beta_{1,k}c_1c_{k,0} = \gamma_{1,k}c_{k+1,0} \tag{22}$$

and setting $c_{1,0} = c_1$. Eq. (20) can now be written as

$$\begin{aligned} I_k &= \beta_{1,k}c_1c_k - \beta_{1,k}\frac{c_{1,0}c_{k,0}}{c_{k+1,0}}c_{k+1} \\ &= \beta_{1,k}c_1c_{k,0}\left(\frac{c_k}{c_{k,0}} - \frac{c_{k+1}}{c_{k+1,0}}\right)\,, \end{aligned}$$

which can be rearranged to

$$\frac{I_k}{\beta_{1,k}c_1c_{k,0}} = \frac{c_k}{c_{k,0}} - \frac{c_{k+1}}{c_{k+1,0}}\,. \tag{23}$$

From Eq. (21), it follows that all fluxes $I_k$ are equal in steady-state. In particular, all the fluxes are equal to the nucleation rate $J$, which is defined as the flux from the critical size $n^*$ to the size $n^* + 1$. Substituting $J$ for $I_k$ and summing both sides of Eq. (23) over all cluster sizes up to some big number $N$ gives

$$\begin{aligned} J\sum_{k=1}^{N}\frac{1}{\beta_{1,k}c_1c_{k,0}} &= \frac{c_1}{c_{1,0}} - \frac{c_2}{c_{2,0}} + \frac{c_2}{c_{2,0}} - \cdots - \frac{c_{N-1}}{c_{N-1,0}} + \frac{c_{N-1}}{c_{N-1,0}} - \frac{c_N}{c_{N,0}} \\ &= 1 - \frac{c_N}{c_{N,0}}\,, \end{aligned} \tag{24}$$

where the ratio of steady-state and "constrained equilibrium" concentrations at size $N$ still needs to be solved in order to calculate the nucleation rate.

Based on the detailed balance condition (22), the "constrained equilibrium" cluster concentrations have a power law dependence

$$c_{k,0} = \left(\prod_{j=1}^{k-1}\frac{\beta_{1,j}}{\gamma 1,j}\right)c_1^k \tag{25}$$

31

on the monomer concentration. If the stability of the clusters increases with increasing size so that $\gamma_{1,k}/(c_1\beta_{1,k}) < a$ for some number $a < 1$ and all values of $k$ beyond some size, it follows from Eq. (25) that $c_{N,0} \to \infty$ when $N \to \infty$. On the other hand, assuming that in steady-state the net flux is dominated by collisions ($\gamma_{1,k}c_{k+1} \ll \beta_{1,k}c_1c_k$) for all values of $k$ beyond some size, the steady-state concentrations of large clusters are approximately $c_k \approx J/(c_1\beta_{1,k})$. If the collision rates increase with increasing size, or at least decrease slower than $1/c_{k,0}$, it follows that $c_N/c_{N,0} \to 0$ as $N \to \infty$. Taking the limit $N \to \infty$ in Eq. (24) then yields the expression

$$J = \left( \sum_{k=1}^{\infty} \frac{1}{\beta_{1,k}c_1c_{k,0}} \right)^{-1} \tag{26}$$

for the steady-state nucleation rate in terms of the "constrained equilibrium" cluster concentrations.

Going back to Eq. (25), the derivatives of the "constrained equilibrium" concentrations with respect to the monomer concentration are

$$\left( \frac{\partial c_{k,0}}{\partial c_1} \right)_T = k\frac{c_{k,0}}{c_1} \, ,$$

when the temperature and thereby the collision and evaporation rates defining the concentrations $c_{k,0}$ are kept constant. The derivative of the nucleation rate (Eq. 26) is

$$
\begin{aligned}
\left( \frac{\partial J}{\partial c_1} \right)_T &= -\left( \sum_{k=1}^{\infty} \frac{1}{\beta_{1,k}c_1c_{k,0}} \right)^{-2} \left[ \sum_{n=1}^{\infty} \frac{-1}{\beta_{1,n}\left(c_1c_{n,0}\right)^2} \left( c_{n,0} + c_1 n\frac{c_{n,0}}{c_1} \right) \right] \\
&= \frac{J}{c_1} \left( \sum_{k=1}^{\infty} \frac{1}{\beta_{1,k}c_1c_{k,0}} \right)^{-1} \sum_{n=1}^{\infty} \frac{n+1}{\beta_{1,n}c_1c_{n,0}} \, ,
\end{aligned}
$$

which can be rewritten in terms of a logarithmic derivative as

$$
\begin{aligned}
\left( \frac{\partial \log J}{\partial \log c_1} \right)_T &= \frac{\sum_{n=1}^{\infty} \frac{n+1}{\beta_{1,n}c_1c_{n,0}}}{\sum_{k=1}^{\infty} \frac{1}{\beta_{1,k}c_1c_{k,0}}} \\
&= \frac{\sum_{n=1}^{\infty} f(n)n}{\sum_{k=1}^{\infty} f(k)} + 1 = \langle n \rangle + 1 \, , \tag{27}
\end{aligned}
$$

where $\langle n \rangle$ is the average of the cluster size $n$ over the distribution $f(n) = 1/(\beta_{1,n}c_1c_{n,0})$.

It should be noted that, so far, the "constrained equilibrium" concentrations have been used simply as a shorthand notation, and the same results can be derived directly in terms of the collision and evaporation coefficients by substituting Eq. (25) into Eq. (23). This approach was first presented by Ford (1997) before McGraw and Wu (2003) introduced the "constrained equilibrium" concentrations.

**Connecting the slope to the energy profile**

If the evaporation rates are properties of the clusters and independent of the surrounding vapor as assumed in Section 2.3, they can be solved from the detailed balance condition applied to any equilibrium distribution. The evaporation rate of a monomer from the $(n+1)$-molecule cluster is (see Eqs. 12–16)

$$\gamma_{1,n} = \beta_{1,n} \frac{p^{\ominus}}{k_{\mathrm{B}}T} \exp\left(\frac{G_{n+1}^{\ominus} - G_n^{\ominus} - G_1^{\ominus}}{k_{\mathrm{B}}T}\right) , \tag{28}$$

where the $G^{\ominus}$'s are the Gibbs free energies of the three species, $p^{\ominus}$ is the reference pressure at which the free energies are evaluated, $k_{\mathrm{B}}$ is the Boltzmann constant, and $T$ is the temperature. Inserting Eq. (28) into Eq. (25) and using the ideal gas law for the monomer concentration, the "constrained equilibrium" concentrations can be written as

$$
\begin{aligned}
c_{n,0} &= c_1^n \prod_{j=1}^{n-1}\left[\frac{k_{\mathrm{B}}T}{p^{\ominus}}\exp\left(-\frac{G_{j+1}^{\ominus} - G_j^{\ominus} - G_1^{\ominus}}{k_{\mathrm{B}}T}\right)\right] \\
&= c_1\left(\frac{p_1}{k_{\mathrm{B}}T}\right)^{n-1}\left(\frac{k_{\mathrm{B}}T}{p^{\ominus}}\right)^{n-1}\exp\left(-\frac{G_n^{\ominus} - nG_1^{\ominus}}{k_{\mathrm{B}}T}\right) \\
&= c_1\exp\left(-\frac{G_{n,c_1} - nG_{1,c_1}}{k_{\mathrm{B}}T}\right) = c_1\exp\left(-\frac{\Delta G_{n,c_1}}{k_{\mathrm{B}}T}\right) ,
\end{aligned}
\tag{29}
$$

where the third and fourth equalities, respectively, result from transforming the Gibbs free energies from pressure $p^{\ominus}$ to pressure $p_1 = k_{\mathrm{B}}Tc_1$ as

$$G_{i,c_1} = G_i^{\ominus} - k_{\mathrm{B}}T\log\left(\frac{p_1}{p^{\ominus}}\right)^i ,$$

and denoting the Gibbs free energy of formation of the $n$-molecule cluster from monomers as $\Delta G_n = G_n - nG_1$.

If the Gibbs free energy of formation has one high and narrow global maximum at the critical size $n^*$, and the size dependence of the collision rate constant $\beta_{1,n}$ is not very strong, the function

$$f(n) = (\beta_{1,n}c_1c_{n,0})^{-1} = (\beta_{1,n}c_1^2)^{-1}\exp\left(\frac{\Delta G_{n,c_1}}{k_{\mathrm{B}}T}\right)$$

33

introduced in Eq. (27) will peak even more strongly than the formation free energy at the critical size $n^*$. If this is the case, the term corresponding to the critical cluster size will dominate the sums in Eq. (27), leading to the one-component nucleation theorem

$$\left(\frac{\partial \log J}{\partial \log c_1}\right)_T \approx n^* + 1 \,.$$

The theorem has also been generalized for some special cases of multicomponent nucleation by McGraw and Wu (2003) and McGraw and Zhang (2008). **Paper IV** presents in detail another derivation of the multicomponent nucleation theorem with a different set of assumptions, as well as a discussion of these assumptions.

### 3.2.2 The reality of slope analysis

While slope analysis seems, at a first glance, like a powerful and easy-to-use tool, it is important to keep in mind the details of the derivation of the nucleation theorem. Along the way, several very drastic approximations and assumptions are made. First and foremost, it is assumed that there are no external losses and no coagulation to big particles. This simplification leads to the nucleation theorem not being valid in practically any realistic situation, the possible exceptions being cases like expansion chamber experiments where extremely high nucleation rates can be achieved.

If the effect of external losses can be argued to be negligible in some specific situation, the derivation still contains several other problematic assumptions. The clusters are assumed to grow solely by the addition of single molecules, while for instance in sulfuric acid–driven particle formation, a large fraction of sulfuric acid molecules are expected to be clustered with one or more water molecules and there is no reason to believe that these small clusters would not participate in particle formation and growth. The formation free energy curve, or for multicomponent nucleation the formation free energy curve along the formation pathway, is assumed to have one high maximum that dominates the summation in Eq. (27). Based on quantum chemical calculations, it seems plausible that the formation energy curve may instead have several local maxima and that several cluster sizes can have non-negligible contributions to the summation as discussed in **Paper IV**.

Even assuming that the nucleation theorem would, in principle, be valid in some given situation, there are some practical problems to be overcome before employing

34

it. First of all, the nucleation rate is not a directly measurable quantity. What can be measured is the particle concentration in a specific size range or above some cutoff size. If the main assumptions of the nucleation theorem are valid, namely there are no external losses and no coagulation (that is, no collisions where neither of the collision partners is a monomer), the nucleation rate can be obtained directly as the time derivative of the particle concentration above some given size. Otherwise, calculating the nucleation rate requires further assumptions and approximations as well as knowledge about the external losses and the particle growth rate. As the growth rate cannot be measured directly or obtained reliably from concentration measurements (Olenius et al., 2014), an accurate determination of the nucleation rate is also not possible. Furthermore, there are several other technical problems related to determining the slope of the nucleation rate, keeping the monomer concentrations of all but one of the precursor compounds constant between experiments, measuring the monomer concentrations, and achieving a steady-state in nucleation experiments. These issues are discussed in detail in **Paper IV**.

Due to all the above-mentioned technical and fundamental problems, slope analysis, while seemingly convenient, cannot be considered a useful tool for analyzing experimental data and extracting information about cluster properties. However, as the only information that the nucleation theorem would yield even in an ideal situation is the approximate size and composition of the critical cluster, discarding this tool is not a very big loss. While knowing the size of the critical cluster can be interesting in its own right and even give some vague idea of the dynamics of the system, it does not give any detailed information about the energetics or time scale of the cluster formation process.

## 3.3 Fitting rate constants to produce observed cluster concentrations

Sections 3.1 and 3.2 present data analysis methods developed for special idealized situations: equilibrium or steady-state conditions, respectively, and no external losses. Both methods are based on an intricate theoretical framework, and as most of the work is done in the derivation of the method, they are in practice very simple to use.

35

When analyzing cluster distributions in complicated, non-ideal situations, such easy-to-use, previously-derived tools are not available, and each case must be treated as a separate problem. What needs to be done is to develop a model for calculating cluster concentrations based on precursor concentrations and rate constants, and fit this model to observed cluster distributions (Figure 4). While this approach is more difficult to implement than those discussed earlier, it also has one great advantage. It can, at least in principle, be used to solve any number of rate constants for any set of clusters using measurements from any kind of experimental setup.
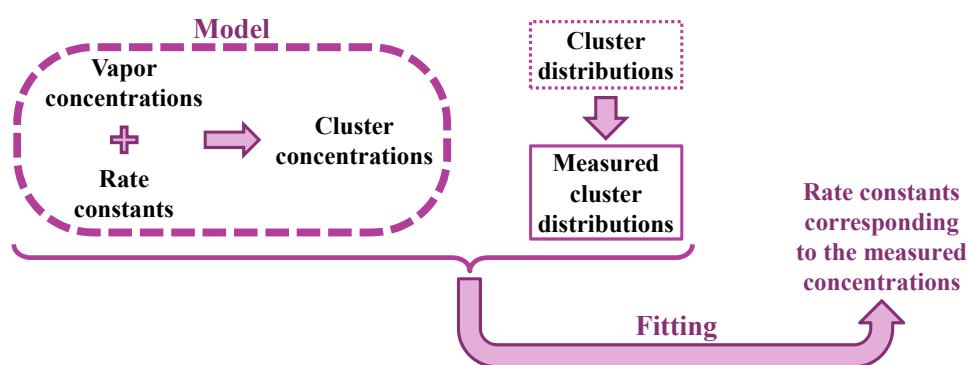


Figure 4: Outline of the process for estimating cluster collision and evaporation rates by combining a cluster formation model with concentration measurements.

### 3.3.1 Case studies based on traditional optimization methods

A simple but case-specific approach for solving rate constants from concentration measurements was introduced by Bzdek et al. (2010a). They studied the substitution of one base molecule type by another in small positively charged acid–base clusters (the acid being sulfuric acid or nitric acid and the base being ammonia, methylamine, dimethylamine or trimethylamine), and measured the concentrations of different cluster types as a function of time. Each experiment started by the mass-selection of clusters of a specific composition, and these were let to react with a high vapor concentration of one base compound. The authors solved analytically the differential equations describing the time evolution of the cluster concentrations to get an expression for the concentration of each cluster type as a function of time. The reaction rates were treated as free parameters, and their values were optimized to find a best fit to the measured concentrations.

Each experiment dealt with a maximum of five cluster types, corresponding to four substitution reaction rates to be fitted. The fitting was done using the simplex method, and a reasonably close agreement was found between the measured and optimized theoretical concentrations. In later similar experiments focusing on larger sulfuric acid–base clusters (Bzdek et al., 2010b), positively charged methanesulfonic acid–base clusters (Bzdek et al., 2011b) and negatively charged sulfuric acid–base clusters (Bzdek et al., 2011a), decomposition of some clusters was observed to compete with the studied base-substitution reactions. The assumed simple reaction scheme was, therefore, not strictly valid, but still described the system closely enough that the discrepancy was found not to affect significantly the kinetic analysis.

Jen et al. (2014) took a step towards analyzing more complicated situations. They used a flow tube to study the formation of neutral clusters from sulfuric acid and base vapors, the base being either ammonia, methylamine, dimethylamine or trimethylamine. A Cluster CIMS (a nitrate ion chemical ionization mass spectrometer; Eisele and Hanson, 2000; Hanson and Eisele, 2002; Zhao et al., 2010) was used to detect sulfuric acid molecules and different clusters containing up to two sulfuric acid molecules. The $HSO_4^-$ ion signal was converted into a concentration of neutral sulfuric acid molecules, possibly clustered with water and base molecules, and the $H_2SO_4 \cdot HSO_4^-$ ion signal was converted into the summed concentration of all neutral cluster types containing two sulfuric acid molecules and any number of water and base molecules.

As two major precursor compounds (sulfuric acid and a base) were present, and clusters were forming and growing, a detailed description of the process would have led to at least tens of unknown rate constants even neglecting the distribution of different hydration states for each cluster type. Instead of trying to optimize all these parameters, Jen et al. (2014) laid out two simplified cluster formation schemes where the addition of a base molecule could take place either only as a second step after the formation of an unstable pure acid dimer or only as a first step before the second acid molecule was added. In both schemes, all cluster types could also be lost to an external sink. All collision rates were set to a fixed value taken from kinetic gas theory, and most evaporation rates were set to zero. Only two evaporation rates in the first scheme or one in the second scheme were treated as free parameters. Even with these simplifications, the models could not be solved analytically. Instead they were solved numerically both for steady state and for a

time period corresponding to the residence time in the flow tube. The models were fitted to the experimental data separately for each of the four base compounds, and the main qualitative trends of the concentration of two-acid clusters as a function of precursor concentrations could be reproduced. However, none of the four models (the two schemes and either steady state or time dependence) could capture all features of the acid and base concentration dependence for all base compounds.

The study of Jen et al. (2014) serves to illustrate a major obstacle encountered when fitting cluster models to experimental data: multidimensional optimization problems are far from trivial, and not having an analytical solution for the time evolution of cluster concentrations makes the fitting even trickier. On the other hand, if the cluster model is simplified in order to have less free parameters, the model might no longer describe the system accurately enough for the fitted parameters to have a clear physical meaning. If the aim is to obtain a predictive tool for calculating cluster concentrations as was the case in the study of Jen et al. (2014), using a simple model can be adequate if it captures all important trends in the data. If, however, the focus is on solving the rate constants, the dynamics of the cluster population needs to be described more accurately.

### 3.3.2  Markov chain Monte Carlo for parameter estimation

Most optimization methods commonly used for multidimensional problems start from some initial guess for the parameter values, take steps in the parameter space aiming to decrease the value of the function to be minimized, and stop when a minimum is found. Starting the algorithm from different initial points may result in finding different local minima, but there is no general way to ensure that the global minimum has been found. This drawback is, to a great extent, resolved in Markov chain Monte Carlo (MCMC) methods.

Like traditional optimization methods, MCMC methods for parameter estimation are also based on taking steps in parameter space. However, the aim is not to move always only toward lower values of the function. In fact, although MCMC methods can be applied to fitting and optimization problems, they are not exclusively optimization algorithms in the sense that they would only give as output the parameter values corresponding to the best fit or global minimum. Instead, they provide the probability distribution of different combinations of parameter values, given the observed data and the probability distribution of measurement

errors. All parameter values through which the algorithm has walked are saved, and the steps are chosen so that the distribution of points in this list converges toward the desired probability distribution.

In the Metropolis algorithm (Metropolis et al., 1953), a random step is taken at each iteration from the old parameter values $\boldsymbol{k}_{\mathrm{old}}$ to some new set of parameter values $\boldsymbol{k}_{\mathrm{new}}$. In this first and most simple Monte Carlo method, a symmetric random walk algorithm is used, meaning that the likelihood $P_{\mathrm{old,new}}$ of choosing a step to $\boldsymbol{k}_{\mathrm{new}}$ when starting from $\boldsymbol{k}_{\mathrm{old}}$ is equal to that of choosing a step leading to $\boldsymbol{k}_{\mathrm{old}}$ when starting from $\boldsymbol{k}_{\mathrm{new}}$. In the case of fitting a cluster formation model to measured concentrations, these parameter values $\boldsymbol{k}_{\mathrm{old}}$ and $\boldsymbol{k}_{\mathrm{new}}$ correspond to possible sets of values for rate constants and other unknown parameters to be determined. These can include for instance collision and evaporation rates, wall loss constants and probabilities for different clusters to fragment in the instrument before detection. Once the new parameter values have been chosen, a cluster formation simulation is performed using these values, and the output concentrations $\boldsymbol{C}_{\mathrm{new}}$ are compared to the measured concentrations $\boldsymbol{C}_{\mathrm{exp}}$. Assuming that the measurement errors of the experimental cluster concentrations are independent and log-normally distributed with variance $\sigma^2$, the likelihood that the new parameters would produce the experimental data is

$$p(\boldsymbol{C}_{\mathrm{exp}} \mid \boldsymbol{k}_{\mathrm{new}}) = \frac{1}{(2\pi\sigma^2)^{n_{\mathrm{data}}}} \exp\left(-\frac{1}{2\sigma^2}SS_{\mathrm{new}}\right), \tag{30}$$

where $n_{\mathrm{data}}$ is the number of experimental data points and

$$SS_{\mathrm{new}} = \sum_{i=1}^{n_{\mathrm{data}}} \left(\log_{10} C_{\mathrm{exp},i} - \log_{10} C_{\mathrm{new},i}\right)^2 \tag{31}$$

is the square sum of the differences between the logarithms of the measured and modeled concentrations. If the new parameter values produce the experimental observations better than the previous values, that is, if $SS_{\mathrm{new}} < SS_{\mathrm{old}}$, the new point is directly accepted into the list of saved points. Otherwise, the point may still be accepted, but with a probability that decreases with increasing $SS_{\mathrm{new}}$. The two cases can be combined into the joint expression

$$\alpha = \min\left(1, \exp\left[-\frac{1}{2}\sigma^{-2}(SS_{\mathrm{new}} - SS_{\mathrm{old}})\right]\right) \tag{32}$$

for the acceptance probability. If the new point is not accepted, the old values $\boldsymbol{k}_{\mathrm{old}}$ are saved again into the list of points as a new entry. Then, a new random

step is taken from whichever point was accepted into the list of parameter values, a new simulation is performed, the new point is either accepted or rejected, and the process is repeated over and over again.

If the algorithm for taking the random steps is ergodic, that is, if any point in parameter space can be reached in a finite number of steps starting from any other point, it has been shown by Metropolis et al. (1953) that the list of saved parameter values converges toward the distribution

$$\pi(\boldsymbol{k_i}) \propto \exp\left(-\frac{1}{2\sigma^2} SS_i\right) , \tag{33}$$

which has the same form as $p(\boldsymbol{C}_{\mathrm{exp}} \mid \boldsymbol{k_i})$ defined in Eq. (30). This can be illustrated by considering a large ensemble of systems where a random walker is moving along the parameter space according to the Metropolis algorithm. If the numbers of walkers currently located at $\boldsymbol{k_i}$ and $\boldsymbol{k_j}$ are $\nu_i$ and $\nu_j$, respectively, and $SS_i > SS_j$, the number of walkers accepting a step from $\boldsymbol{k_i}$ to $\boldsymbol{k_j}$ is $P_{i,j}\nu_i$, as all steps from $\boldsymbol{k_i}$ to $\boldsymbol{k_j}$ are accepted. In the opposite direction, $SS$ increases and only a fraction of the attempted steps are accepted. The number of walkers accepting a step from $\boldsymbol{k_j}$ to $\boldsymbol{k_i}$ is $P_{j,i}\nu_j \exp[-1/(2\sigma^2)(SS_i - SS_j)]$. As the likelihood $P_{i,j}$ of attempting a step from $\boldsymbol{k_i}$ to $\boldsymbol{k_j}$ is assumed to be symmetric with respect to $i$ and $j$, the net flux from $\boldsymbol{k_i}$ to $\boldsymbol{k_j}$ is

$$\begin{aligned} f_{i \to j} &= P_{i,j}\nu_i - P_{j,i}\nu_j \exp\left[-\frac{1}{2}\sigma^{-2}(SS_i - SS_j)\right] \\ &= P_{i,j}\nu_j \left[\frac{\nu_i}{\nu_j} - \frac{\pi(\boldsymbol{k_i})}{\pi(\boldsymbol{k_j})}\right] . \end{aligned} \tag{34}$$

If $\nu_i/\nu_j > \pi(\boldsymbol{k_i})/\pi(\boldsymbol{k_j})$, there is a net flux toward $\boldsymbol{k_j}$, and if $\nu_i/\nu_j < \pi(\boldsymbol{k_i})/\pi(\boldsymbol{k_j})$ the net flux is in the opposite direction. In both cases, the ensemble moves toward the distribution defined in Eq. (33).

Assuming that cluster formation can be described adequately with birth-death equations, MCMC parameter estimation is an extremely powerful tool for inferring rate constants from cluster formation experiments. It performs well even for problems with tens of unknown parameters, and not having an analytical expression for the cluster concentrations is not a problem. In addition to collision and evaporation rates, also other unknown parameters such as the detection efficiencies of different clusters or their fragmentation probabilities inside an instrument can be determined. The method was tested in **Paper V** by solving evaporation

rates from simulated cluster distributions where the values for all parameters are known, and for most of the reactions along the main formation pathway these correct values could be retrieved from the analysis. MCMC was also applied to steady-state concentrations of negatively charged sulfuric acid–ammonia clusters measured in the CLOUD chamber (Olenius et al., 2013b), but there were not enough experimental data points available to get unambiguous estimates for all parameters. This setback, in fact, points out the one big weakness in MCMC parameter estimation: it requires an extensive amount of input data. Getting collision rates from the data analysis in addition to the evaporation rates was not even attempted, as this would have required information about the time scale of the cluster formation process instead of only steady-state distributions. Ideally, all precursor concentrations should be varied widely and measured accurately, and the time dependence of the precursor and cluster concentrations should be recorded over the whole experiment.

While the MCMC analysis applied to the measured cluster concentrations in **Paper V** did not yet provide a clear picture of which clusters are stable and what their main formation pathways are, it gave some new insight into the process of analyzing cluster distribution measurements. First, several very different combinations of values for the evaporation rates were observed to yield an equally good agreement with the measured concentrations. This implies that finding some model that reproduces well a limited set of cluster concentration measurements does not necessarily mean that it is the correct model describing the true dynamics of the cluster population. The second major finding was that fragmentation of clusters in the APi-TOF mass spectrometer seems to affect strongly the shape of the measured cluster distribution as suggested earlier by Adamov et al. (2013).

# 4 Review of papers and the author's contribution

**Paper I** presents simulations of ammonia-to-dimethylamine substitution in small positively charged and electrically neutral sulfuric acid–ammonia clusters. Thermochemical data for the clusters are also presented. The simulation related to positive clusters shows good agreement with a previously published experiment. A comparison between the positively charged and electrically neutral cases points out how strongly the properties and dynamics of clusters are affected by the charging state. I performed most of the quantum chemical calculations, wrote the code for simulating the base substitution processes, performed the simulations and wrote the paper.

**Paper II** studies the formation of sulfuric acid–dimethylamine clusters. Most of the paper is devoted to measurements performed in the CLOUD chamber at CERN, and the results are complemented with cluster dynamics simulations performed with the Atmospheric Cluster Dynamics Code (ACDC). Dimethylamine is observed to enhance cluster formation much more strongly than ammonia, and neutral cluster formation is noted to dominate over ionic pathways. The experimental results and simulations are in qualitative agreement. I participated in developing ACDC, performed most of the ACDC simulations, wrote parts of the model description in the Supplementary Information and commented on the manuscript.

**Paper III** investigates the charging of sulfuric acid and sulfuric acid–dimethylamine clusters by nitrate ions in the chemical ionization mass spectrometer (CIMS). The charging process is simulated using the ACDC, and new thermochemical data are presented for some of the clusters. The paper also presents a comparison of three different quantum chemical methods and two different parameterizations of ion-neutral collision rates. I came up with the research idea, participated in developing ACDC, performed the quantum chemical calculations and cluster kinetics simulations and wrote the paper.

**Paper IV** examines the applicability of the nucleation theorem in non-ideal situations. The derivation of the nucleation theorem is reviewed in detail, and the required assumptions and their validity are discussed. ACDC is used for simulating the nucleation rate of a multicomponent system in cases where one or more of the assumptions are not valid, and the appropriate partial derivatives of the

nucleation rate are compared to the size and composition of the critical cluster. The nucleation theorem is seen to fail badly in all remotely realistic situations. I participated in planning the study, developed a detailed derivation for the multicomponent nucleation theorem, performed and interpreted part of the ACDC simulations and wrote a major fraction of the paper.

**Paper V** introduces a Monte Carlo approach for inferring evaporation rates and fragmentation probabilities from cluster distribution measurements. The method is first tested on simulated concentration distributions of negatively charged sulfuric acid–ammonia clusters, and it is shown to give reasonably accurate estimates for many of the input rate constants. The method is then applied to experimental data, but due to the limited number of experiments, an unambiguous solution is not reached. Instead, several different sets of parameter values leading to the correct cluster concentrations are found. I developed a Fortran version of ACDC, wrote a program for performing Monte Carlo simulations, performed the simulations, analyzed the results and wrote the paper.

# 5 Accomplished goals and future perspectives

During the time spent on the work presented in this Thesis, modeling tools for studying cluster formation have taken a big leap forward. Collision rates from classical physics and cluster energies from quantum chemistry have been combined with cluster kinetics modeling, and for the first time a qualitative, if not quite quantitative, agreement has been achieved between experimental and theoretical cluster concentrations (**Paper I**, Olenius et al., 2013b) and formation rates (**Paper II**). While the accuracy of cluster formation energies can still be improved by using more sophisticated quantum chemistry methods and more data can be computed for different clusters, the basic framework is now ready.

The focus is, therefore, shifting from the development of simulation tools and comparisons between modeling and experiments to a wider variety of applications for cluster formation simulations. **Papers III–V** illustrate some of these new directions.

One big problem when comparing simulations and measurements is that the quantities that are compared are not always equivalent, or the model does not take into account all details of the experiment. For instance, what is called the sulfuric acid monomer concentration in experimental studies, is actually likely to correspond to the signal from sulfuric acid monomers as well as all clusters containing one sulfuric acid molecule and any number of water and base molecules (**Paper III**). Furthermore, these clusters might have a higher detection efficiency than the plain monomers and thus contribute more to the measured sulfuric acid concentration than the sulfuric acid monomer itself. **Paper III** only focuses on one part of one instrument, the chemical ionization chamber, and on a few molecules and clusters. A similar chemical ionization study has also been performed for positive charging of base molecules with protonated acetone (Ruusuvuori et al., 2014). In the future, also other instruments such as the Particle Size Magnifier (Vanhanen et al., 2011) should be investigated using cluster formation simulations. Incorporating detailed cluster population modeling into a classical fluid dynamics simulation as was done by Panta et al. (2012) will improve significantly the comparability between flow tube experiments and cluster formation simulations.

The issue of comparing quantities that are defined differently in different contexts is also related to the second focus area in future applications for cluster population

simulations: reviewing data analysis methods commonly applied to experimental data. One example is the slope analysis method discussed in **Paper IV**. Another instance is the detailed analysis of discrepancies between different definitions for growth rates by Olenius et al. (2014). A similar task would be to evaluate how well the simulated particle formation rates defined as a flux across some size limit correspond to formation rates determined from cluster concentrations using the tools typically applied to experimental data. In addition to evaluating data analysis methods, cluster kinetics simulations can also be used to evaluate the accuracy of condensation models often applied to study particle growth.

A third big theme in future applications for cluster formation simulations is the use of MCMC parameter estimation to determine rate constants and other not directly measurable parameters related to cluster formation and cluster measurements (**Paper V**). A big challenge in advancing the use of MCMC methods in this context is that big enough data sets are not commonly available. Although a large number of similar experiments are often performed, all results from each of these are seldom reported, as this would not be informative for most readers. Instead, the data is analyzed with some suitable tools and published in a way that best illustrates the findings. However, this way the data is typically not detailed enough to be suitable for MCMC parameter estimation. Therefore, the best way to proceed is by close collaboration between experimentalists and modelers.

Besides focusing on the applications mentioned above, also some new features could still be incorporated into cluster formation simulations. So far, the only reactions that have been included in ACDC are proton transfers, and even those are described in a rather cursory way: the protons are always on the molecules where it is energetically most favorable to have them, and any molecules can evaporate from the clusters regardless of their protonation state. In the future, evaluating whether this approach is sensible and possibly modifying it, and on the other hand also enabling other chemical reactions in the cluster-phase might be useful.

From a more theoretical point-of-view, one future challenge is to look into the assumption that each collision results immediately in the minimum-energy configuration of the formed cluster. It might be necessary to find a way to take into account that after a cluster is formed, its evaporation rate may vary with time as it rearranges toward a more favorable configuration and loses or gains energy in collisions with air molecules.

# References

Adamov, A., Junninen, H., Duplissy, J., Sipilä, M., Kulmala, M., and CLOUD collaboration (2013). Cluster measurements at CLOUD using a high resolution ion mobility spectrometer-mass spectrometer combination. *AIP Conference Proceedings*, 1527(1):350 – 353.

Arnold, F., Fabian, R., and Joos, W. (1981). Measurements of the height variation of sulfuric acid vapor concentrations in the stratosphere. *Geophys. Res. Lett.*, 8(3):293 – 296.

Barker, R. A. and Ridge, D. P. (1976). Ion–polar neutral momentum transfer collision frequencies: A theoretical approach. *J. Chem. Phys.*, 64(11):4411 – 4416.

Becke, A. D. (1993). Density-functional thermochemistry. III. The role of exact exchange. *J. Chem. Phys.*, 98(7):5648 – 5652.

Becker, R. and Döring, W. (1935). Kinetische Behandlung der Keimbildung in übersättigten Dämpfen. *Annalen der Physik*, 416(8):719 – 752.

Bork, N., Du, L., and Kjaergaard, H. G. (2014a). Identification and Characterization of the HCl–DMS Gas Phase Molecular Complex via Infrared Spectroscopy and Electronic Structure Calculations. *J. Phys. Chem. A*, 118(8):1384 – 1389.

Bork, N., Du, L., Reiman, H., Kurtén, T., and Kjaergaard, H. G. (2014b). Benchmarking Ab Initio Binding Energies of Hydrogen-Bonded Molecular Clusters Based on FTIR Spectroscopy. *J. Phys. Chem. A*, 118(28):5316 – 5322.

Brown, P., Byrne, G., and Hindmarsh, A. (1989). VODE: A Variable-Coefficient ODE Solver. *SIAM J. Sci. and Stat. Comput.*, 10(5):1038 – 1051.

Bzdek, B. R., DePalma, J. W., Ridge, D. P., Laskin, J., and Johnston, M. V. (2013). Fragmentation Energetics of Clusters Relevant to Atmospheric New Particle Formation. *J. Am. Chem. Soc.*, 135:3276 – 3285.

Bzdek, B. R., Ridge, D. P., and Johnston, M. V. (2010a). Amine exchange into ammonium bisulfate and ammonium nitrate nuclei. *Atmos. Chem. Phys.*, 10:3495.

Bzdek, B. R., Ridge, D. P., and Johnston, M. V. (2010b). Size-Dependent Reactions of Ammonium Bisulfate Clusters with Dimethylamine. *J. Phys. Chem. A*, 114(43):11638 – 11644.

Bzdek, B. R., Ridge, D. P., and Johnston, M. V. (2011a). Amine reactivity with charged sulfuric acid clusters. *Atmos. Chem. Phys.*, 11(16):8735 – 8743.

Bzdek, B. R., Ridge, D. P., and Johnston, M. V. (2011b). Reactivity of methanesulfonic acid salt clusters relevant to marine air. *J. Geophys. Res. Atmos.*, 116(D3):D03301.

Chesnavich, W. J., Su, T., and Bowers, M. T. (1980). Collisions in a noncentral field: A variational and trajectory investigation of ion–dipole capture. *J. Chem. Phys.*, 72(4):2641 – 2655.

Cox, R. A. (1973). Some experimental observations of aerosol formation in the photo-oxidation of sulphur dioxide. *J. Aerosol Sci*, 4(6):473 – 483.

DePalma, J. W., Bzdek, B. R., Ridge, D. P., and Johnston, M. V. (2014). Activation Barriers in the Growth of Molecular Clusters Derived from Sulfuric Acid and Ammonia. *J. Phys. Chem. A*, 118(49):11547 – 11554.

DePalma, J. W., Bzdek, B. R., Ridge, D. P., and Johnston, M. V. (2015). Correction to "Activation Barriers in the Growth of Molecular Clusters Derived From Sulfuric Acid and Ammonia". *J. Phys. Chem. A*, 119(5):931 – 932.

Doyle, G. J. (1961). Self-Nucleation in the Sulfuric Acid-Water System. *J. Chem. Phys.*, 35(3):795 – 799.

Dugan, J. V. and Magee, J. L. (1967). Capture Collisions between Ions and Polar Molecules. *J. Chem. Phys.*, 47(9):3103 – 3112.

Dunning, Jr, T. H., Peterson, K. A., and Wilson, A. K. (2001). Gaussian basis sets for use in correlated molecular calculations. X. The atoms aluminum through argon revisited. *J. Chem. Phys.*, 114(21):9244 – 9253.

Ehn, M., Junninen, H., Schobesberger, S., Manninen, H. E., Franchin, A., Sipilä, M., Petäjä, T., Kerminen, V.-M., Tammet, H., Mirme, A., Mirme, S., Hõrrak, U., Kulmala, M., and Worsnop, D. R. (2011). An Instrumental Comparison of Mobility and Mass Measurements of Atmospheric Small Ions. *Aerosol Sci. Technol.*, 45(4):522 – 532.

Eisele, F. and Tanner, D. (1993). Measurement of the gas phase concentration of $H_2SO_4$ and methane sulfonic acid and estimates of $H_2SO_4$ production and loss in the atmosphere. *J. Geophys. Res.*, 98(D5):9001 – 9010.

Eisele, F. L. and Hanson, D. R. (2000). First Measurement of Prenucleation Molecular Clusters. *J. Phys. Chem. A*, 104(4):830 – 836.

Elm, J., Bilde, M., and Mikkelsen, K. V. (2013). Assessment of binding energies of atmospherically relevant clusters. *Phys. Chem. Chem. Phys.*, 15(39):16442 – 16445.

Farkas, L. (1927). Keimbildungsgeschwindigkeit in übersättigten Dämpfen. *Zeitschr. f. physik. Chemie*, 125:236 – 242.

Ford, I. J. (1997). Nucleation theorems, the statistical mechanics of molecular clusters, and a revision of classical nucleation theory. *Phys. Rev. E*, 56(5):5615–5629.

Franchin, A., Ehrhart, S., Leppä, J., Nieminen, T., Gagné, S., Schobesberger, S., Wimmer, D., Duplissy, J., Riccobono, F., Dunne, E., Rondo, L., Downard, A., Bianchi, F., Kupc, A., Tsagkogeorgas, G., Lehtipalo, K., Manninen, H. E., Almeida, J., Amorim, A., Wagner, P. E., Hansel, A., Kirkby, J., Kürten, A., Donahue, N. M., Makhmutov, V., Mathot, S., Metzger, A., Petäjä, T., Schnitzhofer, R., Sipilä, M., Stozhkov, Y., Tomé, A., Kerminen, V.-M., Carslaw, K., Curtius, J., Baltensperger, U., and Kulmala, M. (2015). Experimental investigation of ion-ion recombination at atmospheric conditions. *Atmospheric Chemistry and Physics Discussions*, 15(3):3667 – 3702.

Froyd, K. and Lovejoy, E. (2012). Bond Energies and Structures of Ammonia–Sulfuric Acid Positive Cluster Ions. *J. Phys. Chem. A*, 116(24):5886 – 5899.

Froyd, K. D. and Lovejoy, E. R. (2003a). Experimental Thermodynamics of Cluster Ions Composed of $H_2SO_4$ and $H_2O$. 1. Positive Ions. *J. Phys. Chem. A*, 107(46):9800 – 9811.

Froyd, K. D. and Lovejoy, E. R. (2003b). Experimental Thermodynamics of Cluster Ions Composed of $H_2SO_4$ and $H_2O$. 2. Measurements and ab Initio Structures of Negative Ions. *J. Phys. Chem. A*, 107(46):9812 – 9824.

Fuchs, N. A. and Sutugin, A. G. (1965). Coagulation rate of highly dispersed aerosols. *J. Colloid Sci.*, 20(6):492 – 500.

Ge, X., Wexler, A. S., and Clegg, S. L. (2011). Atmospheric amines - Part I. A review. *Atmos. Environ.*, 45(3):524 – 546.

Gioumousis, G. and Stevenson, D. P. (1958). Reactions of Gaseous Molecule Ions with Gaseous Molecules. V. Theory. *J. Chem. Phys.*, 29(2):294 – 299.

Gupta, S. K., Jones, E. G., Harrison, A. G., and Myher, J. J. (1967). Reactions of thermal energy ions. VI. Hydrogen-transfer ion–molecule reactions involving polar molecules. *Can. J. Chem.*, 45(24):3107 – 3117.

Hanson, D. R. and Eisele, F. (2000). Diffusion of $H_2SO_4$ in Humidified Nitrogen: Hydrated $H_2SO_4$. *J. Phys. Chem. A*, 104(8):1715 – 1719.

Hanson, D. R. and Eisele, F. L. (2002). Measurement of prenucleation molecular clusters in the $NH_3$, $H_2SO_4$, $H_2O$ system. *J. Geophys. Res.*, 107(D12):AAC 10–1.

Hanson, D. R. and Lovejoy, E. R. (2006). Measurement of the Thermodynamics of the Hydrated Dimer and Trimer of Sulfuric Acid. *J. Phys. Chem. A*, 110(31):9525 – 9528.

Hättig, C. and Weigend, F. (2000). CC2 excitation energy calculations on large molecules using the resolution of the identity approximation. *J. Chem. Phys.*, 113(13):5154 – 5161.

Hippler, M. (2007). Quantum chemical study and infrared spectroscopy of hydrogen-bonded CHCl3–NH3 in the gas phase. *J. Chem. Phys.*, 127(8):084306.

Hiraoka, K. and Kebarle, P. (1975). Energetics, stabilities, and possible structures of $CH_5^+(CH_4)_n$ clusters from gas phase study of equilibriums $CH_5^+(CH_4)_{n-1} + CH_4 = CH_5^+(CH_4)_n$ for $n = 1$–5. *J. Am. Chem. Soc.*, 97(15):4179 – 4183.

Hogg, A. M., Haynes, R. M., and Kebarle, P. (1966). Ion-Solvent Molecule Interactions Studied in the Gas Phase. Heats and Entropies of Individual Steps. $NH_4^+ \cdot (n-1)NH_3 + NH_3 = NH_4^+ \cdot nNH_3$. *J. Am. Chem. Soc.*, 88(1):28 – 31.

Hogg, A. M. and Kebarle, P. (1965). Mass-Spectrometric Study of Ions at Near-Atmospheric Pressure. II. Ammonium Ions Produced by the Alpha Radiolysis of Ammonia and Their Solvation in the Gas Phase by Ammonia and Water Molecules. *J. Chem. Phys.*, 43(2):449 – 456.

IPCC (2013). *Climate Change 2013: The Physical Science Basis. Contribution of Working Group I to the Fifth Assessment Report of the Intergovernmental Panel on Climate Change.* Stocker, T.F., Qin, D., Plattner, G.-K., Tignor, M., Allen, S.K., Boschung, J., Nauels, A., Xia, Y., Bex, V. and Midgley, P.M. (eds.). Cambridge University Press, Cambridge, United Kingdom and New York, NY, USA.

Israël, H. (1970). *Atmospheric Electricity, vol. I.* Israel Program for Sci. Transl. & NSF, Jerusalem.

Jen, C. N., McMurry, P. H., and Hanson, D. R. (2014). Stabilization of sulfuric acid dimers by ammonia, methylamine, dimethylamine, and trimethylamine. *J. Geophys. Res. Atmos.*, 119(12):7502 – 7514.

Jokinen, T., Sipilä, M., Junninen, H., Ehn, M., Lönn, G., Hakala, J., Petäjä, T., Mauldin, III, R. L., Kulmala, M., and Worsnop, D. R. (2012). Atmospheric sulphuric acid and neutral cluster measurements using CI-APi-TOF. *Atmos. Chem. Phys.*, 12:4117 – 4125.

Junninen, H., Ehn, M., Petäjä, T., Luosujärvi, L., Kotiaho, T., Kostiainen, R., Rohner, U., Gonin, M., Fuhrer, K., Kulmala, M., and Worsnop, D. R. (2010). A high-resolution mass spectrometer to measure atmospheric ion composition. *Atmos. Meas. Tech.*, 3:1039 – 1053.

Kashchiev, D. (1982). On the relation between nucleation work, nucleus size, and nucleation rate. *J. Chem. Phys.*, 76(10):5098 – 5102.

Kebarle, P. and Hogg, A. M. (1965). Heats of Hydration and Solvation by Mass Spectrometry. *J. Chem. Phys.*, 42(2):798 – 799.

Kiang, C. S., Stauffer, D., Mohnen, V. A., Bricard, J., and Vigla, D. (1973). Heteromolecular nucleation theory applied to gas-to-particle conversion. *Atmos. Environ.*, 7(12):1279 – 1283.

Kummerlöwe, G. and Beyer, M. K. (2005). Rate estimates for collisions of ionic clusters with neutral reactant molecules. *Int. J. Mass Spectrom.*, 244(1):84 – 90.

Kurtén, T., Kuang, C., Gómez, P., McMurry, P. H., Vehkamäki, H., Ortega, I. K., Noppel, M., and Kulmala, M. (2010). The role of cluster energy nonaccommodation in atmospheric sulfuric acid nucleation. *J. Chem. Phys.*, 132(2):024304.

Langevin, M. P. (1905). Une formule fondamentale de théorie cinétique. *Annales de chimie et de physique*, 5:245 – 288.

Leverentz, H. R., Siepmann, J. I., Truhlar, D. G., Loukonen, V., and Vehkamäki, H. (2013). Energetics of Atmospherically Implicated Clusters Made of Sulfuric Acid, Ammonia, and Dimethyl Amine. *J. Phys. Chem. A*, 117(18):3819 – 3825.

López-Yglesias, X. and Flagan, R. C. (2013). Ion–Aerosol Flux Coefficients and the Steady-State Charge Distribution of Aerosols in a Bipolar Ion Environment. *Aerosol Sci. Technol.*, 47(6):688 – 704.

Loukonen, V., Bork, N., and Vehkamäki, H. (2014a). From Collisions to Clusters: First Steps of Sulfuric Acid Nanocluster Formation Dynamics. *Mol. Phys.*, 112(15):1979 – 1986.

Loukonen, V., Kuo, I.-F. W., McGrath, M. J., and Vehkamäki, H. (2014b). On the stability and dynamics of (sulfuric acid) (ammonia) and (sulfuric acid) (dimethylamine) clusters: A first-principles molecular dynamics investigation. *Chem. Phys.*, 428(0):164 – 174.

Marlow, W. H. (1980). Derivation of aerosol collision rates for singular attractive contact potentials. *J. Chem. Phys.*, 73(12):6284 – 6287.

McGraw, R. and Wu, D. T. (2003). Kinetic extensions of the nucleation theorem. *J. Chem. Phys.*, 118(20):9337 – 9347.

McGraw, R. and Zhang, R. (2008). Multivariate analysis of homogeneous nucleation rate measurements. Nucleation in the p-toluic acid/sulfuric acid/water system. *J. Chem. Phys.*, 128(6):064508.

Merikanto, J., Zapadinsky, E., Lauri, A., and Vehkamäki, H. (2007). Origin of the Failure of Classical Nucleation Theory: Incorrect Description of the Smallest Clusters. *Phys. Rev. Lett.*, 98(14):145702.

Metropolis, N., Rosenbluth, A. W., Rosenbluth, M. N., Teller, A. H., and Teller, E. (1953). Equation of State Calculations by Fast Computing Machines. *J. Chem. Phys.*, 21(6):1087 – 1092.

Mirabel, P. and Katz, J. L. (1974). Binary homogeneous nucleation as a mechanism for the formation of aerosols. *J. Chem. Phys.*, 60(3):1138 – 1144.

Mohnen, V. A. (1970). Preliminary results on the formation of negative small ions in the troposphere. *Journal of Geophysical Research*, 75(9):1717 – 1721.

Montgomery, Jr, J. A., Frisch, M. J., Ochterski, J. W., and Petersson, G. A. (1999). A complete basis set model chemistry. VI. Use of density functional geometries and frequencies. *J. Chem. Phys.*, 110(6):2822 – 2827.

Moran, T. F. and Hamill, W. H. (1963). Cross Sections of Ion–Permanent-Dipole Reactions by Mass Spectrometry. *J. Chem. Phys.*, 39(6):1413 – 1422.

Munson, M. S. B. and Field, F. H. (1966). Chemical Ionization Mass Spectrometry. I. General Introduction. *J. Am. Chem. Soc.*, 88(12):2621 – 2630.

Nielsen, A. E. (1964). *Kinetics of Precipitation.* International Series of Monographs in Analytical Chemistry, Vol. 18. Pergamon Press, Oxford.

Olenius, T., Kupiainen-Määttä, O., Ortega, I. K., Kurtén, T., and Vehkamäki, H. (2013a). Free energy barrier in the growth of sulfuric acid-ammonia and sulfuric acid-dimethylamine clusters. *J. Chem. Phys.*, 139(8):084312.

Olenius, T., Riipinen, I., Lehtipalo, K., and Vehkamäki, H. (2014). Growth rates of atmospheric molecular clusters based on appearance times and collision–evaporation fluxes: Growth by monomers. *J. Aerosol Sci*, 78:55 – 70.

Olenius, T., Schobesberger, S., Kupiainen-Määttä, O., Franchin, A., Junninen, H., Ortega, I. K., Kurtén, T., Loukonen, V., Worsnop, D. R., Kulmala, M., and Vehkamäki, H. (2013b). Comparing simulated and experimental molecular cluster distributions. *Faraday Discuss.*, 165(0):75–89.

Ortega, I. K., Kupiainen, O., Kurtén, T., Olenius, T., Wilkman, O., McGrath, M. J., Loukonen, V., and Vehkamäki, H. (2012). From quantum chemical formation free energies to evaporation rates. *Atmos. Chem. Phys.*, 12:225 – 235.

Ortega, I. K., Olenius, T., Kupiainen-Määttä, O., Loukonen, V., Kurtén, T., and Vehkamäki, H. (2014). Electrical charging changes the composition of sulfuric acid–ammonia/dimethylamine clusters. *Atmos. Chem. Phys.*, 14:7995 – 8007.

Paasonen, P., Olenius, T., Kupiainen, O., Kurtén, T., Petäjä, T., Birmili, W., Hamed, A., Hu, M., Huey, L. G., Plass-Duelmer, C., Smith, J. N., Wiedensohler, A., Loukonen, V., McGrath, M. J., Ortega, I. K., Laaksonen, A., Vehkamäki, H., Kerminen, V.-M., and Kulmala, M. (2012). On the formation of sulphuric

acid - amine clusters in varying atmospheric conditions and its influence on atmospheric new particle formation. *Atmos. Chem. Phys.*, 12:9113 – 9133.

Panta, B., Glasoe, W. A., Zollner, J. H., Carlson, K. K., and Hanson, D. R. (2012). Computational Fluid Dynamics of a Cylindrical Nucleation Flow Reactor with Detailed Cluster Thermodynamics. *J. Phys. Chem. A*, 116(41):10122 – 10134.

Partanen, L., Hänninen, V., and Halonen, L. (2012). Ab Initio Structural and Vibrational Investigation of Sulfuric Acid Monohydrate. *J. Phys. Chem. A*, 116(11):2867 – 2879.

Román, C. E. and Garzón, I. L. (1991). Evaporation of Lennard-Jones clusters. *Z. Phys. D: At., Mol. Clusters*, 20(1):163 – 166.

Ruusuvuori, K., Hietala, P., Kupiainen-Määttä, O., Jokinen, T., Junninen, H., Sipilä, M., Kurtén, T., and Vehkamäki, H. (2014). The charging of neutral dimethylamine and dimethylamine-sulphuric acid clusters using protonated acetone. *Atmos. Meas. Tech. Discuss.*, 7(11):11011 – 11044.

Schrödinger, E. (1926). Quantisierung als Eigenwertproblem (Erste Mitteilung). *Annalen der Physik*, 384(4):361 – 376.

Shampine, L. and Reichelt, M. (1997). The MATLAB ODE Suite. *SIAM J. Sci. Comp.*, 18(1):1 – 22.

Shugard, W. J., Heist, R. H., and Reiss, H. (1974). Theory of vapor phase nucleation in binary mixtures of water and sulfuric acid. *J. Chem. Phys.*, 61(12):5298 – 5304.

Sihto, S.-L., Kulmala, M., Kerminen, V.-M., Maso, M. D., Petäjä, T., Riipinen, I., Korhonen, H., Arnold, F., Janson, R., Boy, M., Laaksonen, A., and Lehtinen, K. E. J. (2006). Atmospheric sulphuric acid and aerosol formation: Implications from atmospheric measurements for nucleation and early growth mechanisms. *Atmos. Chem. Phys.*, 6:4079 – 4091.

Stinson, J. L., Kathmann, S. M., and Ford, I. J. (2016). A classical reactive potential for molecular clusters of sulphuric acid and water. *Mol. Phys.*, 114(2):172 – 185.

Su, T. and Bowers, M. T. (1973). Theory of ion-polar molecule collisions. Comparison with experimental charge transfer reactions of rare gas ions to geometric isomers of difluorobenzene and dichloroethylene. *J. Chem. Phys.*, 58(7):3027.

Su, T. and Chesnavich, W. J. (1982). Parametrization of the ion-polar molecule collision rate constant by trajectory calculations. *J. Chem. Phys.*, 76(10):5183 – 5185.

Vanhanen, J., Mikkilä, J., Lehtipalo, K., Sipilä, M., Manninen, H. E., Siivola, E., Petäjä, T., and Kulmala, M. (2011). Particle Size Magnifier for Nano-CN Detection. *Aerosol Sci. Technol.*, 45(4):533 – 542.

Viggiano, A. A. and Arnold, F. (1981). Extended sulfuric acid vapor concentration measurements in the stratosphere. *Geophys. Res. Lett.*, 8(6):583 – 586.

Volmer, M. and Weber, A. (1926). Keimbildung in übersättigten Gebilden. *Z. Phys. Chem.*, 119:277 – 301.

Weber, R. J., McMurry, P. H., Eisele, F. L., and Tanner, D. J. (1995). Measurement of Expected Nucleation Precursor Species and 3–500-nm Diameter Particles at Mauna Loa Observatory, Hawaii. *Journal of Atmospheric Sciences*, 52:2242 – 2257.

Weerasinghe, S. and Amar, F. G. (1991). Is cluster evaporation statistical? A comparison of simulation results for Ar13 with exact classical phase space theory. *Z. Phys. D: At., Mol. Clusters*, 20(1):167 – 171.

Wilkening, M. (1985). Characteristics of atmospheric ions in contrasting environments. *Journal of Geophysical Research: Atmospheres*, 90(D4):5933 – 5935.

Yasuoka, K. and Matsumoto, M. (1998). Molecular dynamics of homogeneous nucleation in the vapor phase. I. Lennard-Jones fluid. *J. Chem. Phys.*, 109(19):8451 – 8462.

Yu, F. (2005). Quasi-unary homogeneous nucleation of $H_2SO_4$-$H_2O$. *J. Chem. Phys.*, 122(7):074501.

Yu, F. (2006). Effect of ammonia on new particle formation: A kinetic $H_2SO_4$-$H_2O$-$NH_3$ nucleation model constrained by laboratory measurements. *J. Geophys. Res. Atmos.*, 111(D1):D01204.

Zhao, J., Eisele, F. L., Titcombe, M., Kuang, C., and McMurry, P. H. (2010). Chemical ionization mass spectrometric measurements of atmospheric neutral clusters using the clusterCIMS. *J. Geophys. Res.*, 115(D8):D08205.